Master Thesis

Truncation of the zebrafish E3 ubiquitin ligase and co-chaperone Chip leads to increased disorganisation of Purkinje cell dendrites and an altered heat shock response

Johanna Letzner

June 2022

Master of Science in Biology -

Developmental Biology, Physiology and Nutrition

Department of Biological Sciences, University of Bergen, Norway

Acknowledgements

This project was conducted at the University of Bergen and supported by the Western Norway Health Authorities, Helse Vest's Open Research Grant (grant #912250).

For the help on this project I would like to thank Yasaman Pakdaman for her previous work on the project and for her help during the first weeks in the lab. I would further like to thank my supervisor Associate Professor Ståle Ellingsen, and co-supervisor Dr. Elsa Denker for their continuous guidance and valuable advice. Thank you for all the motivation and just the right amount of pressure that helped me finish this project.

I would also like to give a special thanks to Kristin Foss Telstø for being a true companion along the road, without whom I most likely would not have been able to finish this project. Thank you for all the laughs, I truly appreciate all the (sometimes exhausting) hours we spent together in the lab.

I would also like to thank my family and friends for the encouragement and for keeping me sane during the process. Lastly I want to thank the entire staff at MDB for being so very welcoming and for including us students in their social events. I feel lucky to have been a part of their work environment.

Bergen, 01.06.2022

Johanna Letzner

Contents

Abstract **4**

1 Introduction **8**

1.1 Neurodegenerative diseases 8

1.1.1 Cerebellar Ataxia - SCAR16 8

1.1.2 STUB1 encodes CHIP 9

1.2 The Mechanisms of Maintaining Proteostasis 10

1.2.1 General Principles of the Ubiquitin-Proteasome System 11

1.2.2 The UPS in Neurodegenerative Diseases 12

1.2.3 CHIPs Function in the UPS 13

1.3 The Heat Shock Response 13

1.3.1 The Heat Shock Proteins 14

1.3.2 Heat Shock Factor 1 15

1.3.3 General Mechanisms of the HSR 16

1.4 The Zebrafish as a Model for Neurodegeneration 17

1.4.1 The Cerebellum 18

1.4.2 CRISPR-Cas Methodology 19

1.4.3 The *stub1* Knockout Mutant 20

2 Aim and Perspective of Study **21**

3 Materials and Methods **22**

3.1 Handling and breeding fish 22

3.1.1 Maintenance 22

3.1.2 Breeding 22

3.2 Genotyping 22

3.2.1 Tail Cuts and genomic DNA extraction 22

3.2.2 Amplification of genomic DNA by PCR 23

3.2.3 Restriction enzyme digestion of PCR product 24

3.2.4 Agarose gel electrophoresis 25

3.3 Immunohistochemistry 25

3.3.1 Euthanasia and fixation 26

3.3.2 Dissection and cryopreservation . . . 26
3.3.3 Embedding and Sectioning . . . 26
3.3.4 Antibody staining . . . 26
3.4 Imaging of IHC stained sections . . . 27
3.5 Image analysis . . . 27
3.6 Cerebellum Measurements . . . 28
3.6.1 Cerebellum Size . . . 28
3.6.2 Purkinje Cell abundance . . . 28
3.7 Heat shock experiment design . . . 29
3.7.1 Hatching and survival . . . 29
3.7.2 Sampling for RT-qPCR . . . 29
3.7.3 Sampling for western blot . . . 29
3.8 RT-qPCR . . . 30
3.8.1 Primer Design . . . 30
3.8.2 RNA extraction and quantification . . . 31
3.8.3 cDNA synthesis . . . 32
3.8.4 RT-qPCR . . . 32
3.8.5 Primer Efficiency and Specificity . . . 33
3.8.6 Relative quantification and statistical analysis . . . 34
3.9 Western Blot on heat shocked Zebrafish Larvae (5dpf) . . . 34
3.9.1 Protein Extraction and Quantification . . . 34
3.9.2 SDS page . . . 35
3.9.3 Immunodetection . . . 35
3.9.4 Protein quantification and statistical analysis . . . 36

4 Results **41**

4.1 Genotyping of fish . . . 41
4.2 Investigating signs of neurodegeneration in 3 year old zebrafish . . . 41
4.2.1 Purkinje cell amount in the cerebellum . . . 44
4.2.2 Dendrite orientation . . . 45
4.3 Heat Shock . . . 46
4.3.1 Transcript levels of *hsf1*, *hsp70*, *hsp90* following heat-shock . . . 46
4.3.2 Protein levels of Hsp70 during heat-shock recovery . . . 56

5 Discussion **58**

5.1 Investigation of the cerebellum and its Purkinje cells 58

5.1.1 Purkinje cell dendrite morphology 59

5.1.2 CHIP in the cerebellum and Purkinje cells 60

5.2 The effect of heat stress on the HSR 62

5.2.1 Hsp90 63

5.2.2 Hsp70 63

5.2.3 Hsf1 64

5.2.4 The importance of the CHIP U-box domain 65

5.3 The effect of environmental factors on the brain and Purkinje cells 66

5.4 Conclusion 68

5.5 Future Prospects 68

A Appendix **81**

A.1 Section selection for Purkinje cell count 81

A.2 Neurotracing reconstructions of all individuals in dendrite orientation analysis 82

A.3 RT-qPCR melting curves for primers and Ct values of all samples 83

Selected Abbreviations

AD = Alzheimer's disease

ARCA = Autosomal recessive cerebellar ataxia

ATP = Adenosine triphosphate

CA = Cerebellar ataxia

Cas9 = CRISPR-associated protein 9

CC = Crista cerebellaris

CCe = Corpus cerebellaris

cDNA = complementary DNA

Ce = Cerebellum

CHIP= C-terminus of HSC70-interacting protein

CNS = Central nervous system

CP = Core particle

CRISPR = Clustered regularly interspaced short palindromic repeats

Ct = Cycle threshold value

DBS = Double strand break

DCN = Deep cerebellar nuclei

DNA = Deoxyribonucleic acid

Dpf = Days post fertilisation

E1 = Ubiquitin-activating enzyme

E2 = Ubiquitin-conjugating enzyme

E3 = Ubiquitin-protein ligase

E4 = Polyubiquitinating enzyme

ER = Endoplasmic reticulum

GABA = gamma-aminobutyric acid

GCL = Granular cell layer

gRNA = Guide RNA

HDR = Homology directed repair

HH = Helical hairpin

HIER = Heat induced epitope retrieval

HKG = House keeping gene

Hpf = Hours post fertilisation

HSE = Heat-shock element

HSF = Heat-shock factor

HSP = Heat-shock protein

HSR = Heat hock response

Hyp = Hypothalamus

IHC = Immunohistochemistry

ILOCA = Idiopathic late-onset cerebellar ataxia

Indel = Insertion or deletion

LCa = Lobus caudalis cerebelli

LTD = Long term depression

MAS = Multiple system atrophy

ML = Molecular layer

MO = Medulla oblongata

MPTP = 1-methyl-4-phenyl-1,2,3,6-tetrahydropyridine

mRNA = messenger RNA

MT = Microtubule

ND = Neurodegenerative disease

NHEJ = Non-homologous end joining

NPC = Nuclear pore complex

NTC = Non-template control

o/n = Over night

OB = Olfactory bulb

PAM = Protospacer adjacent motif

PCL = Purkinje cell layer

PCR = Polymerase chain reaction

PD = Parkinson's disease

PQC = Protein quality control

PTM = Post-transcriptional modification

Pvalb = Parvalbumin

RING = Really interesting new gene

RNA = Ribonucleic acid

ROS = Reactive oxygen species

RT = Room temperature

RT-qPCR = Real time quantitative polymerase chain reaction

SCA = Spinocerebellar ataxia

SCAR16 = Spinocerebellar ataxia recessive type 16

SCA48 = Spinocerebellar ataxia type 48

Stub1 = STIP1 homology and U-box containing protein 1

Tel = Telencephalon

TeO = Tectum opticum

T_m = Melting temperature

TPR = Tetratricopeptide repeat

TSD = Teleost-specific genome duplication

Ub = Ubiquitin

UPS = Ubiquitin-proteasome system

Abstract

Neurodegenerative diseases (NDs) are characterised by neuronal atrophy and loss of motoric, emotional and cognitive functions. Cerebellar ataxias (CAs) affect the cerebellum, which is important in motoric control and fine-tuning. SCAR16 and SCA48 are two CAs associated with mutations in the STIP1-homology and U-box-containing protein 1 *(STUB1)* gene, which codes for the C-terminus of HSC70 interacting protein (CHIP). The ubiquitin-proteasome system (UPS) and the heat shock response (HSR) are two parts of the protein quality control system (PQC), which aims to maintain protein homeostasis (proteostasis) in the cell to avoid apoptosis. CHIP plays a vital role in both the UPS and the HSR by facilitating proteasomal degradation of target proteins. In this study, we analysed the Purkinje cell dendrite branching pattern of homozygous Chip U-box mutants lacking the E3 ligase function. Immunohistochemistry was performed on brain sections from UBOX+/+ and UBOX-/- adult zebrafish to visualise dendritic structures. In addition, we subjected 5 day old larvae to heat shock and performed RT-qPCR to analyse transcript levels of *hsp70, hsp90* and *hsf1* in response to HSR initiation. Hsp70 protein levels were also analysed in heat-shocked and non-heat-shocked UBOX+/+ and UBOX-/- zebrafish by performing western blot.

We found an increase in dendrite disorganisation in the cerebellum of our mutant samples compared to wild-type samples. We also found an increase of *hsp70, hsp90* and *hsf1* transcript following heat-shock, and an elevated level of Hsp70 protein in both the heat-shocked and non-heat-shocked mutant compared to the wild-types. This indicates a prolonged stress in the UBOX-/- mutant, which in the UBOX+/+ samples seems to be terminated faster due to the presence of Chips U-box and E3 ligase function.

1 Introduction

1.1 Neurodegenerative diseases

Neurodegenerative diseases (NDs) that affect the brain can originate both internally and externally. External factors include environmental toxicants, e.g. metals such lead or arsenic or pesticides such as 1-methyl-4-phenyl-1,2,3,6-tetrahydropyridine (MPTP) [1], while internal factors include inherited genetic mutations causing hereditary disorders such as spinocerebellar ataxias (SCAs). Many of these disorders lead to degeneration of neurons, and ultimately cell death. One of the main causes of neurodegeneration is protein aggregation, which has been shown to be a central factor in over 70 diseases. This includes Alzheimer's disease (AD), in which there are extracellular aggregations of Aβ-peptides (derivatives of amyloid proteins that facilitate protein aggregate formation) and Parkinson's disease (PD), in which there is a loss in dopamine-producing neurons and formation of Lewy bodies (nuclear α-synuclein inclusions) [2][3].

1.1.1 Cerebellar Ataxia - SCAR16

One category of NDs are cerebellar ataxias (CAs). CAs are characterised by deficits in motoric control and fine-tuning, impaired cognitive and emotional functionality and speech impairment due to weakness of the speech muscles [4][5]. CAs are either sporadic or hereditary. The sporadic forms can be acquired through a variety of factors, some being alcoholism, exposure to toxicants, heavy metals or infections [6]. Some examples are multiple system atrophy (MAS), which is the most common non-hereditary ataxia, and idiopathic late-onset cerebellar ataxia (ILOCA). Hereditary CAs can be X-linked, dominant or recessive. Autosomal recessive cerebellar ataxias (ARCAs) affect 2.2-7/100 000 people and include a rare early-onset ataxia called spinocerebellar ataxia autosomal recessive type 16 (SCAR16) [2]. SCAR16 symptoms overlap with a large range of other CAs. This makes it hard to define clear lines between the different CAs. SCAR16 is characterised by cerebellar ataxia, cognitive impairment and hypogonadism [7]. Other symptoms can include epilepsy, tremor, dysarthria, myoclonus (quick, involuntary muscle jerk) and type 1 diabetes [8].

So far, 19 mutations have been identified that cause SCAR16, and they are all located in the STIP-homology and U-box containing protein 1 (*STUB1*) gene [2][9]. Heterozygous

mutations in *STUB1* have also been identified as the cause for a late-onset CA called autosomal dominant spinocerebellar ataxia type 48 (SCA48) [7][8]. Contradictory to this is the fact that parents of SCAR16 patients, carriers of a single *STUB1* mutation, can be healthy and lack symptoms [10]. This highlights the importance of research on these diseases, since there is still a lot of uncertainty around the effect that different mutations can have on the disease symptoms.

1.1.2 STUB1 encodes CHIP

STUB1 encodes an E3 ligase and co-chaperone called c-terminus of HSC70-interacting protein (CHIP). In this study, CHIP will generally be used as an acronym for the mammalian (human and rodent) protein, while Chip will be used specifically for zebrafish. The same system will be applied for the HSPs and HSFs. In relevant occasions it will be specified whether studies were done on human, rodent, yeast or zebrafish systems. CHIP is a 35kDa protein that is mainly present in tissues with high metabolic activity, such as skeletal muscle, brain, heart and gonads [11]. CHIPs functionality is conserved amongst metazoans, and the protein contains two main domains (Figure 1.1). The tetratricopeptide repeat (TPR) domain is located at the N-terminus, and it binds to the C-terminus of HSP70/HSP90 and other chaperones. The U-box domain at the C-terminus functions as an E3 ligase, ubiquitinating and targeting substrates such as misfolded proteins for degradation. Between these lies the central helical hairpin (HH) region, which facilitates dimerisation [12]. Monomers of CHIP have been found to be inactive, and proper functionality of CHIP is therefore dependant on dimerisation via the HH region [13]. The asymmetric homodimer that forms has only one functional U-box, as the other U-box domain is blocked by a TPR domain in the process [14].

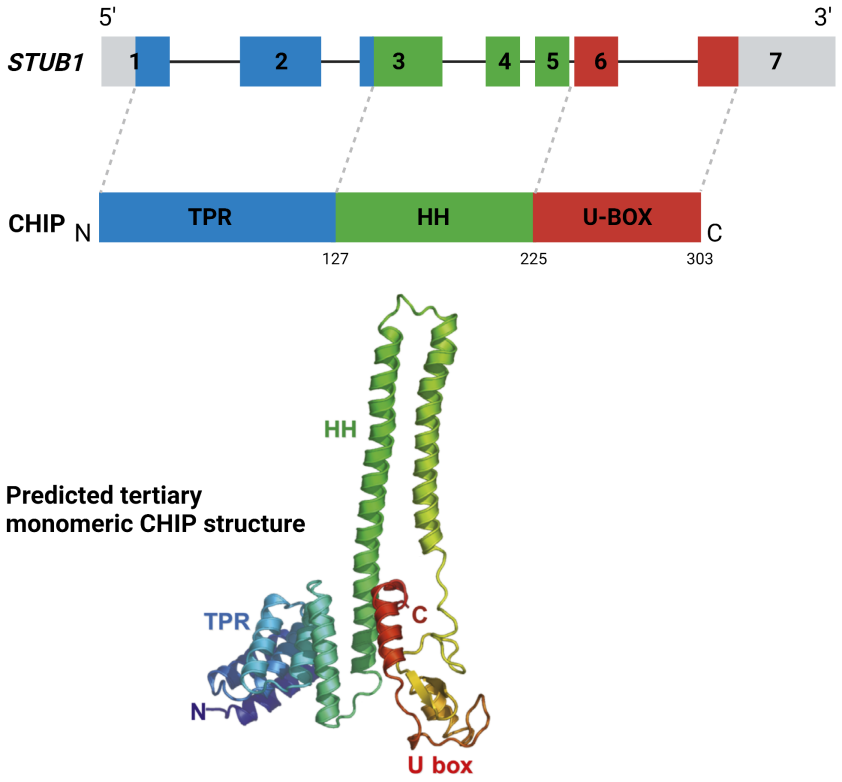

Figure 1.1: ***STUB1 mRNA and CHIP protein structures.*** *Human STUB1 mRNA consists of 7 exons. Grey zones represent UTRs. The human CHIP protein has one TPR domain at its N terminus (blue), one central helical hairpin region (green) and a U-box domain at the C terminus (red). The predicted tertiary 3D structure of the monomeric protein is adapted from Zhang et al. [15].*

1.2 The Mechanisms of Maintaining Proteostasis

Proteome homoeostasis (proteostasis) is the regulation to maintain a functional set of proteins in the cell and thereby assuring overall cellular homeostasis. Cells are constantly exposed to different stress factors such as toxicants, heavy metals or heat. These stress factors can influence the stability of native proteins. Improper folding of new proteins, or the damage of existing proteins, can lead to their aggragation [16]. A protein that has a small structural alteration can be enough to initiate aggregation. Exposed hydrophobic residues stabilise the amyloidogenic intermediate that is the state between the native and the non-native protein structures. These intermediates can aggregate and create oligomers called amyloids. Amyloids are not stable and will bind other oligomers and eventually form protofibrils and amyloid-like fibrils, which are aggregates of oligomers and protofibrils, respectively [17].

To avoid these aggregates, which would eventually cause the cell to initiate programmed

cell death (apoptosis), cells have developed a network of coping mechanisms called the protein quality control system (PQC), which maintains proteostasis by refolding or degrading damaged proteins. It consists of two major pathways. The autophagy-lysosome pathway makes up 10-20% of all degradation activity in the mammalian cell. Lysosomes are organelles that degrade both endogenous proteins and extracellular particles (endocytosis) [3][18]. The other 80-90% are made up of the ubiquitin-proteasome system (UPS), which degrades individual proteins in cooperation with a variety of chaperones and co-chaperones [19][18].

1.2.1 General Principles of the Ubiquitin-Proteasome System

The ubiquitin-proteasome system is initiated when an ubiquitin-activation enzyme (E1)(Figure 1.2A) uses ATP to form thioester bonds between itself and the ubiquitin (Ub) molecule. Ub is a small protein, only 67 amino acids long, which forms poly-ubiquitin chains through isopeptide bonds at its lysine residues. The addition of this chain to a protein increases the rate of its degradation by at least a 10-fold [20]. E1 transfers the Ub to a ubiquitin-conjugating enzyme (E2)(1.2B). E3 Ubiquitin ligases receive the Ub (1.2C) and covalently attach it to the target protein (1.2D). E4, another type of enzyme has been proposed to polyubiquitinate target proteins in cooperation with E1, E2 and E3 [21][22]. The poly-ubiquitinated proteins are eventually recognised by the proteasome [20][23][24]. This large 26S enzyme consists of a 20S core particle (CP) flanked by 19S caps. The 19S cap first recognises the polyubiquitin chain, after which the target protein is unfolded, and transported through the CP. The Ubiquitin is removed and nucleotide hydrolysis (addition of water molecules to break chemical bonds) facilitates proteolysis [16].

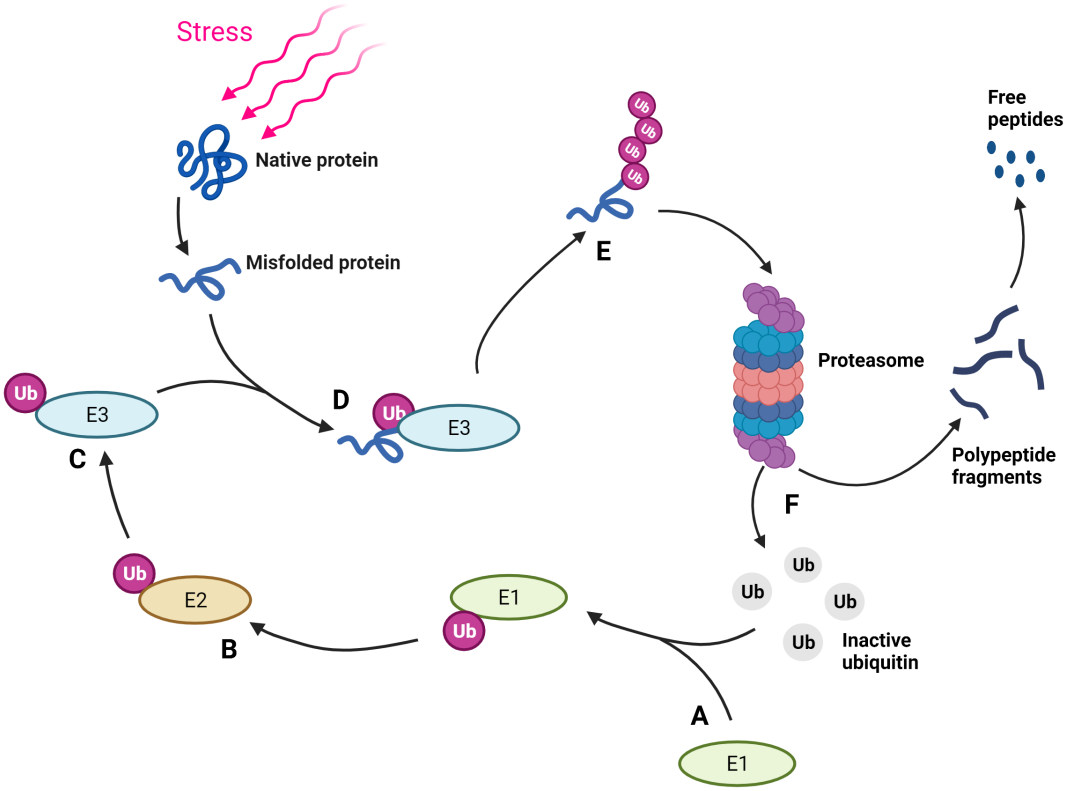

Figure 1.2: ***General illustration of the UPS.*** *Stress factors like heat cause protein degeneration or misfolding. In the UPS, E1 enzymes activate ubiquitin (A) and transfer it to E2 enzymes (B). They in turn transfer the molecule to E3 ligases (C) which attach it to the misfolded protein (D). The poly-ubiquitinated peptide (E) is then recognised by the proteasome and degraded to peptide fragments. Inactive ubiquitin emerges (F). Generated with BioRender.com.*

1.2.2 The UPS in Neurodegenerative Diseases

In NDs, the toxic accumulation of protein aggregates has been shown to originate in a malfunction of the pathways maintaining proteostasis. As mentioned earlier, the UPS stands for up to 90% of protein degradation in the mammalian cell, and it is therefore no surprise that several NDs have been associated with improper UPS function. In some types of AD for example, a mutation in the ubiquitin molecule that prevents the E3 ligase from attaching it to the target protein causes aggregation [25]. Another example is PD, of which there are several different types. Some are initiated by oxidative stress that leads to accumulation of α-synuclein. α-synuclein is a substrate of the E3 ligase Parkin, and malfunction in Parkin, and thereby loss of α-synuclein degradation, can cause PDs [25][26].

1.2.3 CHIPs Function in the UPS

There are more than 600 E3 ligases, of which most contain either the "Really Interesting New Gene" (RING)-domain, or a RING-like domain [27]. The U-box domain, conserved across eukaryotes, is one such RING-like domain. RING-like domains do not contain the signature cysteine residues known to be conserved in RING domains, but nevertheless possess the same functionality [21]. CHIP thus contains the RING-like U-box domain and facilitates transfer of E2-bound ubiquitin to the target protein in addition to bringing the poly-ubiquitinated target in proximity to the proteasome via its TPR domain [28][12][29]. This is achieved by the formation of electrostatic and hydrophobic interactions between the U-box and a conserved binding motif in E2 enzymes [29].

1.3 The Heat Shock Response

The heat shock response (HSR) is a response mechanism to different stressors. It was first discovered in *Drosophila*, in which chromosomal puffing was a result of heat shock [30]. The mechanism is conserved amongst eukaryotes to maintain proteostasis. Not only heat, but also glucose depletion, overexpression of misfolded proteins or oxidative stress caused by proteotoxic compounds such as heavy metals can initiate the HSR [31][30]. Heat can lead to defects in the cytoskeleton, incorrect localisation of organelles, fragmentation of the ER and Golgi apparatus and decrease in mitochondria and lysosomes. Heat also denatures proteins and exposure of residues that facilitate unspecific aggregation [32]. These non-native proteins are targeted for degradation by the heat shock proteins (HSP). Transcription of the genes coding for HSPs is initiated by heat shock factors (HSF). In mammalian cells this group of transcription factors is made up of HSF1, HSF2, HSF4, HSF5, HSFX and HSFY [33]. Yeast in contrast only contains one version, HSF1 [33]. The conserved functionality of HSF1 is one of the reasons why HSF1 is the most studied member of the HSF family [34]. Another reason is its involvement in NDs and cancer. In some cancers, there is an over-activation of HSF1 due to high mutational rates and hence an increase in protein aggregation [30]. However, the pathway with which HSF1 operates in cancer cells differs from the HSR [35]. Some NDs in contrast seem to be characterised by a remarkably low level of HSF1 [33]. To target the underlying mechanisms behind NDs, namely protein misfolding and aggregation, treatments that activate HSF1 are emerging [36].

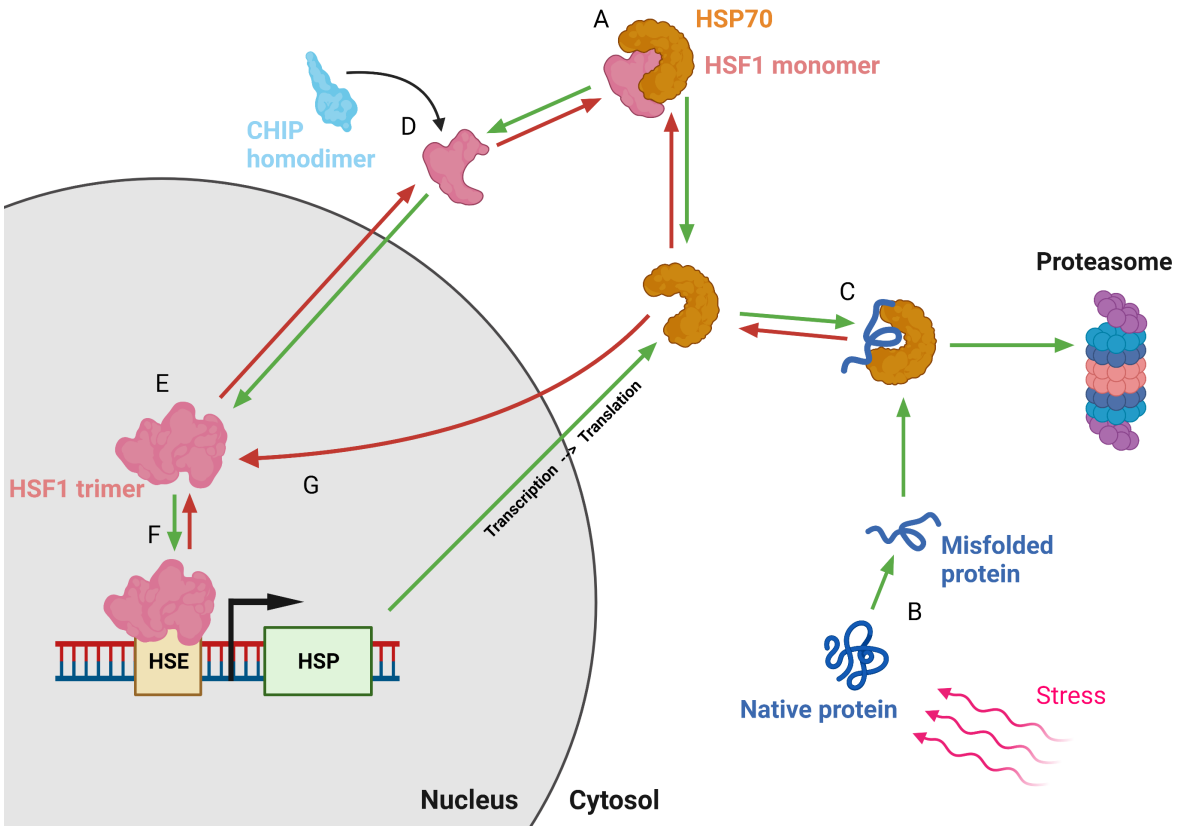

Figure 1.3: ***General simplified illustration of the HSR for HSF1, HSP70 and CHIP.*** *The initiation pathway is shown with green arrows, termination is shown with red arrows. Prior to initiation of the HSR, monomeric HSF1 is bound by HSP70* ***(A)****. The response is initiated by an increasing level of misfolded proteins* ***(B)****. HSP70 disassociates from HSF1 and binds to the target proteins* ***(C)*** *to facilitate degradation by the proteasome. CHIP now binds to HSF1* ***(D)*** *and translocates it into the nucleus, where it trimerises* ***(E)****. Binding of trimeric HSF1 to the HSE initiates HSP70/90 transcription* ***(F)****. When misfolded proteins are degraded, HSP70 translocates into the nucleus and interrupts HSF1 trimerisation to facilitate HSR termination* ***(G)****. HSF1 monomers are then again held inactive by HSP70 binding* ***(A)****. Generated with BioRender.com.*

1.3.1 The Heat Shock Proteins

The heat shock proteins are a group of chaperones that are essential in the prevention of non-native protein accumulation. They target misfolded or denatured proteins to be either refolded or degraded. Refolding by e.g. HSP70 happens in an ATP-dependant manner [37], while protein degradation is mediated by HSP70 and HSP90 through co-chaperone interactions [24]. When the HSR is first initiated, CHIP facilitates an increase in HSP proteins by translocating their transcription factor (HSF1) into the nucleus and

thus initiating HSP transcription. CHIP also ubiquitinates HSPs in the recovery period following stress and, together with other components of the UPS, facilitates HSP degradation [24]. During this recovery period, HSP70 also creates a negative feedback loop for HSP transcription. Newly formed HSP70 rapidly migrates into the nucleus during thermal stress, where it affects the levels of activated HSF1 [38]. Blocking its trimerisation domains, HSP70 (not HSP90) prevents HSF1 from transforming into its active form [33]. All together, HSPs activate the HSR by disassociating from HSF1 and letting it initiate transcription of HSPs. The negative feedback loop comes into play when the HSPs amount exceeds that of the misfolded proteins. HSP70 then terminates the HSR by inhibiting HSF1.

1.3.2 Heat Shock Factor 1

Monomeric HSF1 is at all times present in the cells. This is to ensure rapid response to changes in the cellular environment. Under normal conditions it is kept inactive in its monomeric form by HSP70 and HSP90 [35]. Using the co-chaperone function of its TPR domain, CHIP translocates HSF1 into the nucleus [39]. In addition there is a constant active transport of HSP70-bound HSF1 into- and out of the nucleus via the nuclear pore complex (NPC) [35]. HSF1 transforms into its active form by creating covalent bonds between monomers. In this trimeric form it binds to the heat-shock element (HSE) upstream from the HSP genes. HSEs contain three nGAAn repeats to which each one of the HSF1 monomers binds [33].

There are a lot of mechanisms that control HSF1 activity. This fine-tuning allows for precise responses to various inputs [33][40]. One control mechanism is transcriptional pausing, a process in which the polymerase is paused downstream from the transcription start site. HSF1 was shown to restart transcription by interacting with the polymerase. This process ensures an immediate response to elevated stress levels, as the transcription machinery is already assembled [41]. Post-transcriptional modifications (PTMs) in the form of phosphorylation, acetylation, ubiquitination and SUMOylation further regulate HSF1 activity. Positive regulation by phosphorylation of HSF1 can happen at 73 sites. The addition of phosphate groups increases the negative charge of the protein and increases attraction of the mediator complex, which initiates transcription of HSPs. Though phosphorylation is not essential for activation of HSF1, it increases its transcrip-

tional activity [34]. Another positive regulation is acetylation of specific lysine residues, which increases HSF1 stability. It is thought to protect the protein from degradation by the UPS, sustaining HSF1 activity during cellular stress. Acetylation can also negatively regulate HSF1. Increasing acetylation decreases the DNA binding ability, facilitating downregulation of HSF1 [42]. Another negative regulation is SUMOylation (the addition of Small Ubiquitin-like MOdifier proteins), which is thought to decrease HSF1 activity on a transcriptional level, since other levels of regulatory control, such as trimerisation, DNA-binding and DNA disassociation by HSP70 are not affected by this modulation [33].

1.3.3 General Mechanisms of the HSR

The general mechanisms that drive the HSR are illustrated in Figure 1.3. Stress factors such as heat can cause protein misfolding (1.3B). As a coping mechanism, chaperones such as HSP90 and HSP70 bind to these polypeptides and facilitate degradation by interacting with components of the UPS. Under normal conditions there is enough HSP to both target misfolded proteins and occupy HSF1 (1.3A). But an increase in misfolded proteins causes HSP to disassociate from HSF1 and mediate degradation instead (1.3C). Monomeric HSF1 then translocates into the nucleus (1.3D) where it trimerises (1.3E) and binds to HSEs upstream from the HSP gene (1.3F). These HSE regions are located within the promoter of the HSPs. Transcription is initiated by the recruitment of polymerase II (not shown) and the levels of functional HSP increase.

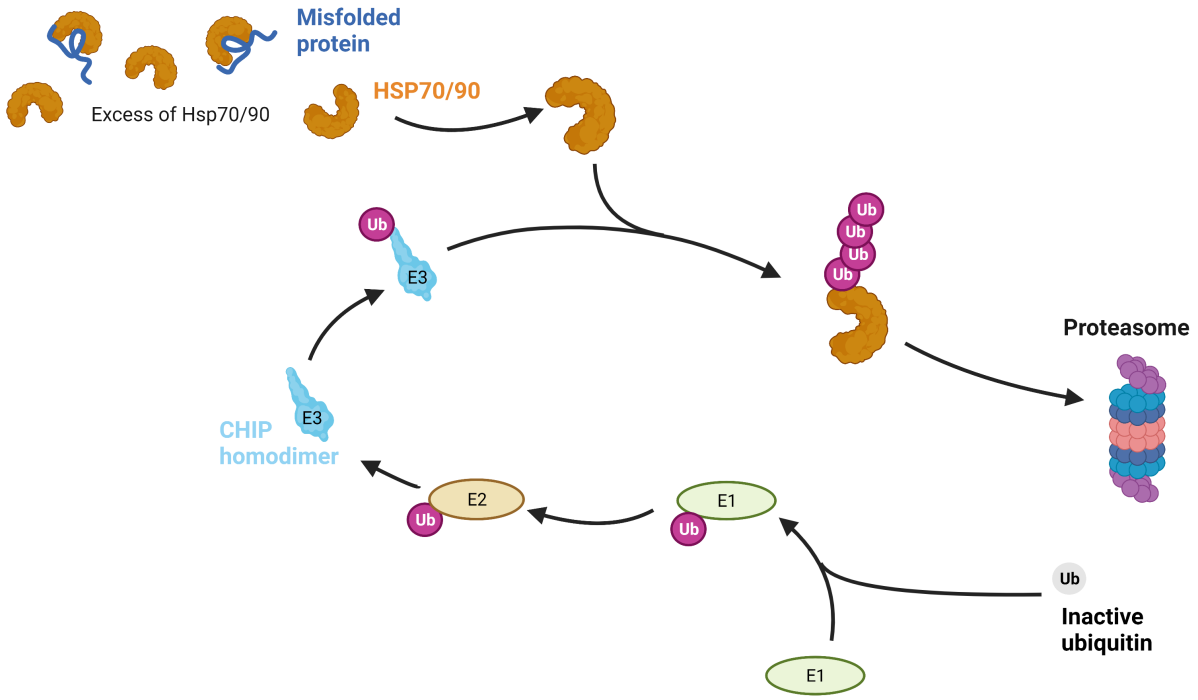

Figure 1.4: Degeneration of HSPs after the HSR. CHIP targets HSPs for proteasomal degradation by ubiquitination (Ub). Inactive Ub is activated by E1 enzymes and transferred to the E3 ligase CHIP by E2 enzymes (see also Figure 1.2).

As proteins are degraded by the HSPs, the level of aggregates decreases as the stress input fades. When there again is a higher level of chaperones than target proteins, HSP70 inhibits HSF1 trimerisation, and thereby stops the HSR. CHIP also contributes to this recovery by degrading HSF1 and HSP70/90 (Figure 1.4). Like it does with its other substrates, CHIP targets the HSPs for degradation by the UPS. If recovery fails, due to for example the failure to terminate transcription of the genes coding for HSPs, and/or failure to degrade HSP proteins, their accumulation will eventually lead to cell death.

1.4 The Zebrafish as a Model for Neurodegeneration

The zebrafish (*Danio rerio*) has become an important model organism in several research fields (development, cancer, organ regeneration, ageing and NDs) [43][44][45][46]. The advancement made with the CRISPR-Cas9 methodology and the sequencing of the zebrafish genome make it easy to create a wide range of mutations in the zebrafish genome [47]. In addition, teleosts (bony fish, to which zebrafish belong) have many similarities with humans. It has been shown that orthologs of at least 84 % of the disease-causing genes found in humans, are present in zebrafish [48]. The zebrafish brain consists of many

of the same structures as the mammalian brain, both on a large scale and at the cellular level. In addition, many cellular mechanisms are conserved amongst teleost and mammalian species [49]. The zebrafish is therefore a good model organism to use for research on diseases or disorders that target the brain. Ataxias often affect the cerebellum, and patients with CAs display difficulties executing motoric tasks originating from cerebellar atrophy [7][50]. The cerebellum is therefore a vital structure that has been investigated in both rodent and zebrafish models [51][52].

1.4.1 The Cerebellum

The cerebellum is a structure located on the dorsal side of the zebrafish brain, between the optic tectum (TeO) anteriorly, and the crista cerebellaris (CC) posteriorly (Figure 1.5A and B). In general, it functions in the fine-tuning of movement, in addition to emotional and cognitive functions. Cerebellar morphology and functionality in zebrafish are strikingly similar to that in humans [53]. Many of the same types of neurons are present in both teleosts and mammals and show many of the same characteristics [54]. Excitatory neurons use glutamate as neurotransmitter, and include granule cells, unipolar brush cells and eurydendroid cells. The inhibitory neurons mostly use gamma-aminobutyric acid (GABA) or glycine as neurotransmitters and include the golgi and the Purkinje cells. The Purkinje cells integrate the information received from a variety of sources and transmit it to the eurydendroid cells (Figure 1.5C). The input comes from pre-cerebellar nuclei, which are located outside of the cerebellum. Their extensions (afferent fibres called climbing and mossy fibers) transmit information to the Purkinje cell dendrites directly, or via granule cells. The molecular layer (ML) of the cerebellum consists of parallel fibres of the granular cells and Purkinje cell dendrites. The parallel fibres create synapses with the Purkinje cell dendrites, which grow in a self-avoidant manner to cover as much space as possible and thereby create a planar structure [55]. The Purkinje cells send their axons (the efferent fibers) to other Purkinje cells or to the eurydendroid cells. These then send the information to different regions of the brain [54][53]. By concentrating all this information and influencing a large range of functions, the Purkinje cells play a critical role in the organism.

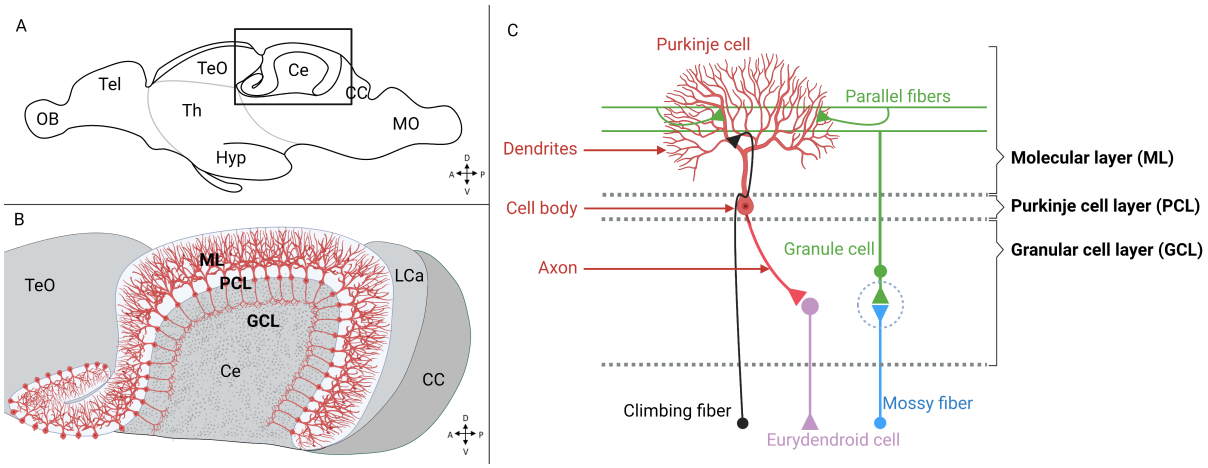

Figure 1.5: Simplified illustration of the zebrafish cerebellum and its neuronal connections. Illustration of whole brain (A), OB: olfactory bulb, Tel: telencephalon, Th: thalamus, TeO: optic tectum, Ce: cerebellum, MO: medulla oblongata, Hyp: hypothalamus and CC: crista cerebellaris. Closer view of cerebellum (B), ML: molecular layer, PCL: Purkinje cell layer and GCL: granular cell layer. Illustration of neuronal connections (C). The cell bodies of the Purkinje cells are located in the PCL. Their dendrites branch out into ML, and receive input from parallel fibres, granular cells and climbing fibres. Mossy fibres transport information towards granular cells. The axons of Purkinje cells extend into the GCL. Eurydendroid cells receive the information and transport it to other regions of the brain. Generated with BioRender.com.

Though the cerebellum is a conserved structure, there are some differences between the human and the zebrafish cerebellum. The mammalian brain lacks eurydendroid cells and instead has deep cerebellar nuclei (DCN) which perform the same task of transmitting signals from Purkinje cell axons to other regions of the brain. In addition, the DCN are located further away from the Purkinje cell layer (PCL) in the mammalian cerebellum than in the teleost cerebellum [53].

1.4.2 CRISPR-Cas Methodology

Being able to edit genomes has always been of interest in fields of medical research and agriculture. The discovery of the CRISPR-Cas9 system has since revolutionised and drastically expanded our possibilities. Model organisms can be easily and effectively mutated to investigate the processes behind diseases like cancer and NDs.

CRISPR is based on the fundamentals of the bacterial immune system consisting of clustered regularly interspaced short palindromic repeats. This system protects the cells against viral infections by editing their own genome to recognise and destroy the viral

RNA. This is achieved with the help of a DNA endonuclease (Cas9) that introduces double-stranded DNA breaks (DSB) in the viral genome. To target the correct site for the introduction of the DNA breaks, a guide RNA (gRNA), which can facilitate RNA-DNA complementary binding, is used as reference. Cas9 then recognises a "CGG" PAM sequence flanking the 3' end of the target (reverse complementary strand shown in yellow in Figure 1.6) and introduces a DSB. The interrupted sequence is then repaired by homology directed repair (HDR) or non-homologous end joining (NHEJ). Variations in these repair mechanisms can introduce changes in the sequence. NHEJ introduces insertions or deletions (indels) that can cause frameshift and gene-knock-out. In HDR, a repair template strand is used to elongate the endogenous DNA strand. This template strand can for example contain a sequence of interest that is to be inserted into the genome [56][57].

1.4.3 The *stub1* Knockout Mutant

The zebrafish U-Box mutant used in this project was created using the CRISPR-Cas system. A target sequence in exon 8 of the *stub1* gene was deleted (red). The 7 base pair (bp) deletion (red arrow in Figure 1.7) resulted in a stop-codon-generating frame shift, which prematurely ends transcription. The U-box domain in the Chip protein (underlined in Figure 1.6, red in Figure 1.7) was thereby truncated.

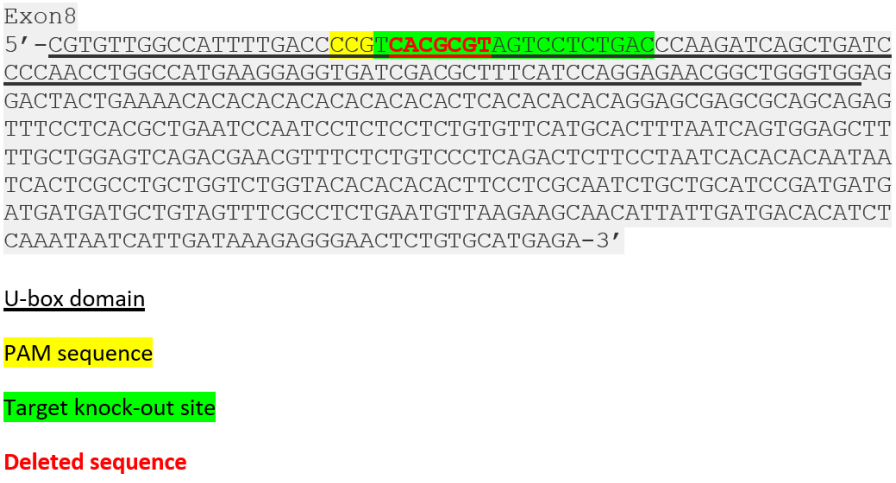

Figure 1.6: ***Overview of exon 8 of stub1 genomic DNA sequence.*** *CRISPR-Cas was used to delete a 7bp sequence (red) in exon 8 of zebrafish stub1. The PAM sequence (yellow) flanking the target site (green) and the U-box domain (underlined) are marked.*

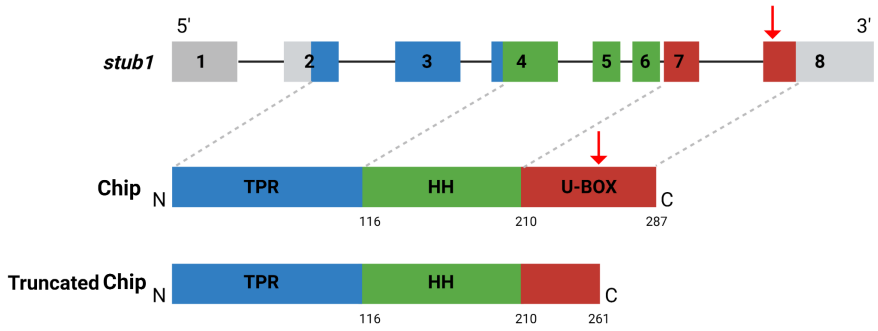

Figure 1.7: ***Zebrafish stub1 and Chip.*** *The zebrafish stub1 gene contains 8 exons and its protein product Chip contains a TPR domain (blue), a U-box domain (red) and a helical hairpin region (green). The CRISPR induced deletion (red arrow) lead to the truncation of the Chip protein.*

Initial behavioural studies of the zebrafish U-box mutants have been done for stages up until 2 years, in which the mutant fish revealed reduced anxiety [52]. Though the opposite behaviour can be seen in patient phenotypes, structural analysis of the cerebellum has shown similarities between U-box mutant zebrafish and human SCAR16 patients, showing cerebellar atrophy and a decrease in Purkinje cell numbers [51].

2 Aim and Perspective of Study

The aim of this study was to expand our understanding of how the truncation of the U-box affects the morphology of the zebrafish Purkinje cells of the cerebellum. NDs are progressive diseases, and it was therefore important to perform cerebellar analysis on older individuals than previously studied. The aim was to study the branching orientation of Purkinje cells, in addition to measuring the cerebellum size and counting the number of Purkinje cell bodies present in the U-box mutant and wild-type cerebellum. In addition, we aimed to investigate how the truncation of Chip U-box domain would influence the HSR. We wanted to measure HSR initiation and recovery by investigating transcript and protein levels of genes/proteins involved in the HSR.

3 Materials and Methods

3.1 Handling and breeding fish

3.1.1 Maintenance

Fish were housed in the zebrafish facility at the Department of Biological Sciences at the University of Bergen in accordance with recommendations from Aleström et al. [58]. All experiments were done in compliance with the Norwegian Animal Welfare Act guidelines, Mattilsynet (FOTS application with FDF reference No. 17/119996).

3.1.2 Breeding

To synchronise mating, a tank with a mesh bottom was used to separate males and females in the same tank. In order to increase the chance of obtaining a high number of fertilised eggs, females and males were kept apart for three days. The eggs were collected the morning of pairing, and kept in E3 medium at 28 °C until maximum 5 days post fertilisation (dpf). Unfertilised eggs and dead embryos/larvae were removed daily.

3.2 Genotyping

3.2.1 Tail Cuts and genomic DNA extraction

DNA was extracted from tail cuts of zebrafish. The fish were anaesthetised in 4% tricaine (in fish water) for 3 min or until gill movement had ceased. 2/3 of the tail fin were cut and suspended in 100µL lysis buffer.

Reagent	Volume	Final concentration
1M Tris-HCl (pH 8.0)	10 μL	100 mM
5M NaCl	4 μL	200 mM
0.5M EDTA (pH 8.0)	1 μL	5 mM
20mg/mL Proteinase K (fresh)(Qiagen, 1114885)	1 μL	200 μg/mL
MilliQ	84μL	
Total reaction volume per sample	100μL	

The samples were incubated at 55-65 °C for 20 min, then vortexed for 1 min. After incubating at 55-65 °C o/n (over night), the samples were again vortexed for 1 min, followed by centrifugation (Eppendorf, 5424R) at max speed (13300 xg) at room temperature (RT) for 2 min. The clear supernatant was collected and 210 μL 100% ethanol were added to each sample. After the tubes were inverted a few times, additional precipitated organic material was carefully removed and the samples incubated on ice for 15 min. The tubes were centrifuged at 4 °C max speed (15000 xg) for 20 min. The supernatant was then carefully discarded, leaving the transparent DNA pellet. To wash the pellet, 210 μL 70% ethanol were added and the samples were centrifuged at 4 °C max speed (15 000 xg) for 10 min. The supernatant was again discarded and the pellets left to air dry at RT (10 min). To dissolve the pellet, 5 μL nuclease free water (Thermo Fisher Scientific, R0582) was added. The samples were then incubated at 55-56 °C for 60 min.

3.2.2 Amplification of genomic DNA by PCR

To amplify the genomic sequences surrounding the CRISPR target (Figure 1.6), a PCR reaction master mix was prepared. The DNA samples were added, and the tubes were mixed with a pipette and spun down before running the PCR program.

Reagent	Volume	Final concentration
10X standard Taq reaction Buffer (NEB, B9014S)	2.5μL	100 mM
10mM dNTPs (NEB, N0447S)	0.5 μL	0.2mM
10μM Forward primer (Sigma)	0.5 μL	0.2μM
10μM Reverse primer (Sigma)	0.5 μL	0.2μM
5U/μL Taq DNA polymerase (Fisher BioReagents, FB-6000-50)	0.125μL	0.2U
MilliQ	15.875μL	
150ng DNA sample	5μL	30ng
Total reaction volume per sample	25μL	

PCR primers:

	Sequence (5' → 3')
Forward	TCTCCATTAATGAGCAGTTGGA
Reverse	ATGAAAGCGTCGATCACCTC

PCR program:

Pre-denaturation	95 °C	3 min	
Denaturation	95 °C	30sec	
Annealing	55 °C	30 sec	x35 cycles
Extension	72 °C	30 sec	
Final extension	72 °C	10 min	
End	4 °C	∞	

3.2.3 Restriction enzyme digestion of PCR product

To identify the CRISPR induced mutation in the DNA sequence (Figure 1.6), a restriction enzyme digestion reaction was prepared and incubated at 37 °C for 30-40 min.

Reagent	Volume	Final concentration
10X CutSmart buffer (NEB, B7206S)	2.5μL	1X
Mlu1-HF restriction enzyme (NEB, R3198L)	0.5μL	0.4 U/μL
PCR product	5 μL	
Total reaction volume per sample	25μL	

Figure 3.1: ***Overview of exon 8 in stub1.*** *The Mlu1 restriction site (red) and PCR primers for genotyping (blue) are marked. The U-box in underlined.*

3.2.4 Agarose gel electrophoresis

To separate the DNA fragments that were cut by the restriction enzyme, a 2.5% 1X TAE agarose gel (SeaKem, 50004)(A9539, Sigma-Aldrich) was prepared. The powder was dissolved by mixing it with the buffer and heating it in the microwave. 10 μL 1X Gelred (Millipore, SCT123) was added from 10000X stock solution, and carefully mixed in, without creating bubbles. The gel was cast, and once it was hardened 25 μL of the samples were loaded after adding 5 μL 6X Purple Loading Dye (Thermo Fisher Scientific, B7024S). The GeneRuler (Thermo Fisher Scientific, SM0331) was used as ladder (1/7 6X Purple Loading Dye, 1/7 GeneRuler, 4/7 Nuclease free water).

3.3 Immunohistochemistry

To visualise Purkinje cells in the cerebellum, immunohistochemistry was performed on zebrafish brain sections. The sections of 3 year old zebrafish were stained for parvalbumin and pictures were taken and analysed to measure cerebellum size, Purkinje cell dendrite orientation, cell-shape and cell-amount.

3.3.1 Euthanasia and fixation

Fish were euthanised in 6-7% Tricain for 2 min and/or until gill movement ceased. They were then kept in ice water for 5 min, and carefully decapitated. The cut was made behind the pectoral fin in order to preserve enough tissue for dissection. The heads were washed in PBS (EMD Milipore, 524650-1EA) and left in 4% paraformaldehyde (PF)(Chemi-Teknik as., 15714-S) in PBS at 4 °C o/n.

3.3.2 Dissection and cryopreservation

The brains were dissected out while pinned onto a styrofoam piece with the dorsal side up. After carefully having scraped off the skin and muscles, tweezers were used to pierce the side of the skull, and the skull was lifted carefully to open a window above the brain. By holding the medulla spinalis with the tweezers and cutting the optical and olfactory nerves on the ventral side, the whole brain could be pulled out carefully. The brains were left in 25% sucrose at 4°C for 24 hours or until they were floating, indicating absorption of the solution.

3.3.3 Embedding and Sectioning

1cm x 1cm aluminium foil moulds were prepared and OCT medium (referred to as just OCT from here on)(Sakura, 4583) poured to cover the bottom. The moulds were left on dry ice until the OCT was almost completely hardened. Then the brain was place inside, with the ventral side facing upwards and covered in OCT. Tweezers were used to hold the brain in place while the OCT hardened. The brains were then stored at -80°C. Sectioning was performed with a Leica CM 3050 cryostat. The sagittal sections were set to be 8 μm thick and collected on Superfrost^{TM}Plus Adhesion Microscope Slides (Epredia, J1800AMNZ). The slides were incubated 10 min at 65°C and then stored at -80 °C until staining.

3.3.4 Antibody staining

Slides were left to thaw at RT for 1h, and dried 10 min at 65 °C. To rehydrate and permeabilise the sections, the slides were washed for 10 min in PBS + 0.05% Triton (PBS-TX)(Sigma, T8787). Slides were stained with mouse-anti-parvalbumin (Pvalb)(1:200)(EMD Milipore, MAB1572) as a primary antibody. The antibody solution was made in blocking

buffer PBS-TX + 1X casein (Sigma, B6429)(PBS-TX-Cas). 200 μL were distributed on each slide and slides were incubated in a humid chamber containing MilliQ (o/n at RT). After the o/n incubation, the primary antibody solution was carefully flushed away with PBS-TX, and the slides were washed 3x15 min in PBS-TX. After washing, the slides were dried carefully around the sections with Whatman paper and Kimtech, and incubated for 45 min in 200 μL secondary antibody solution (1:400 goat anti-mouse AlexaFluor 555 (Thermo Fisher, A32727) in PBS-TX-Cas). Incubation was done in the dark to protect the fluorescence. PBS-TX was used to flush away the solution, and wash the slides 2x5 min (in the dark). To wash away the Triton, they were then washed 3x5 min in PBS. To stain nuclei the slides were mounted in ProLong glass antifade medium containing NucBlue (ThermoFisher, 15858371). The cover slips (#1,5 Menzel-Gläser) were then sealed with nail polish to prevent dehydration.

3.4 Imaging of IHC stained sections

To select the most intact and relevant sections on each slide, they were scanned with a slide scanner (Zeiss Axio Scan.Z1). For each individual, one good section was selected with the aim to study dendrite orientation. The selected slides were then scanned using a confocal microscope (Olypmus FV3000).

3.5 Image analysis

ZEN 3.5 Blue Edition (version 3.5.093.00000) was used to analyse the pictures exported from the slide scanner. They were used for general cerebellum measurements and counting of cells and as reference for further imaging of dendrites with the confocal. Neutube (https://www.neutracing.com/, version 1.0z) was used to create 3D neurotracing models of neurites and color-coding of their branching direction. ImageJ (1.8.0_172) and Photoshop (version 23.2.2.) were used for quantification by analysing the RBG histograms of these pictures. Rstudio (2021.09.1+372) was then used to plot the intensity against the location in the distal part of the cerebellum, to present the directional changes that the dendrites undergo as they branch away form the Purkinje cell bodies.

3.6 Cerebellum Measurements

To evaluate whether the size of the cerebellum differed between mutant and wild-type fish, a range of measurements were undertaken. The thickness of the ML, the whole cerebellum, and the cerebellum and TeO were measured as shown in Figure 3.2. Pictures taken with a slide scanner were used to count the amount of Purkinje cell bodies.

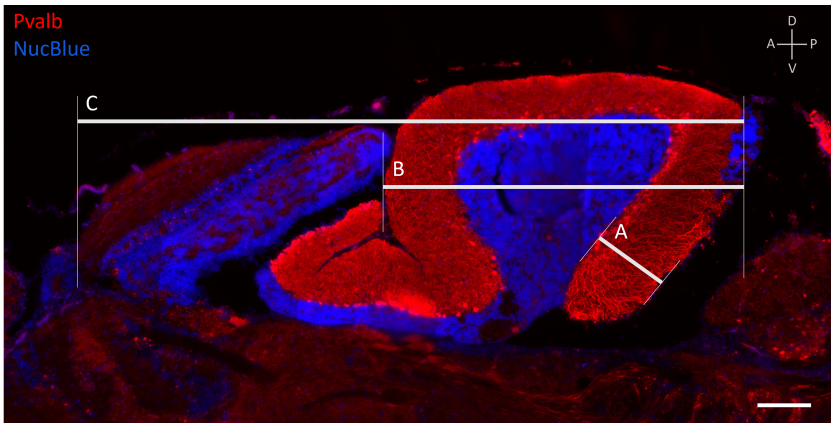

Figure 3.2: ***IHC section of cerebellum showing measurement placement.*** *Pvalb (red) stained brain section, sagittal view. Diameter of ML (A), cerebellum (B) and cerebellum + TeO (C). Scale bar = 200μm.*

3.6.1 Cerebellum Size

The relative proportions of the cerebellum relative were calculated using the following ratios: the thickness of the cerebellum : the diameter of the cerebellum and the TeO and thickness of posterior molecular layer : diameter of the cerebellum. The measurements were done in ZEN 3.5 Blue Edition (version 3.5.093.00000).

3.6.2 Purkinje Cell abundance

The amount of Purkinje cell bodies in the PCL of the cerebellum was determined by manually counting the cell bodies on three sections for each individual (see appendix A.1).

To minimise bias, the section scans were randomised before counting. The number of cells in each individual were then corresponded to the sum of the cells in all three sections and an average for UBOX+/+ and UBOX-/- individuals was calculated.

3.7 Heat shock experiment design

To test the effect of heat-shock on hatching rate, mortality, *hsp* and *hsf1* mRNA and Hs70 protein levels, wild-type and mutant zebrafish larvae were suspended in a water bath (38°C) for 60 min. At the same time, negative controls for both wild-type and mutants were kept at 28°C. All embryos were kept in small glass containers with lids containing 40mL E3 medium.

3.7.1 Hatching and survival

For investigating the hatching pattern, the heat shock was performed on an equal amount of 24 hour old zebrafish wild-type and mutant larvae. The mortality and general developmental progression following heat shock was studied by closely checking the larvae for heartbeat, body size, movement and any morphological abnormalities. This was done throughout the whole observation period, until all larvae had hatched. Hatching usually occurs from 48 hour post fertilisation (hpf), and the embryos were therefore observed from that time point until all eggs were hatched. This was done by counting the hatched larvae every two hours, excluding the hours between 01:00 a.m. and 09:00 a.m. The amount of hatched larvae at a given time point was then plotted to visualise the hatching trend.

3.7.2 Sampling for RT-qPCR

To maximise protein amount, 5 day old embryos were used for the Real Time Quantitative Polymerase Chain Reaction (RT-qPCR) analysis. The were heat shocked as described above, and sampled after a 60 min and 120 min recovery period in a 28 °C water bath. Euthanasia was performed after by placing the containers in ice cold water for 10 min. The embryos were then pooled 20 per Eppendorf tube in six replicates. E3 medium was removed and 150 μL RNAlater (Sigma, MKCH4082) added to each tube. They were kept at 4°C o/n and at -20°C until further use.

3.7.3 Sampling for western blot

For the western blot analysis, 5 dpf old embryos were heat-shocked as described before and sampled after a 60 min recovery period. Euthanasia was performed by placing the containers in ice cold water for 10 min. The embryos were then pooled 40 per Eppendorf

tube in three replicates. E3 medium was removed as much as possible and the tubes were kept on dry ice before storing them at -80 °until further use.

3.8 RT-qPCR

To measure the effect that heat stress had on the heat shock response and the associated proteins, RT-qPCR was run on RNA extracts from 5dpf old zebrafish larvae exposed to a 60 min heat shock.

3.8.1 Primer Design

The introns, exons and complete cDNA sequence for the genes were found on Ensembl (https://www.Ensembl.org). Primer 3 (https://Primer3.ut.ee) was used to identify potential primers, either placed on two different exons or spanning one exon-exon junction (to prevent amplification of genomic DNA). Primer properties were set to be the following: 50-60% GC content, maximum 3 G/C present at 3'end, amplicon size 75-200 bp and a melting temperature (T_m) of 50-65°C. Oligocalc (http://biotools.nubic.northwestern.edu/OligoCalc.html) was used to calculate the T_m of the primers and to check for unwanted hairpin or primer dimer formations. Seaview (http://doua.prabi.fr/software/seaview) was then used to align the primers with the cDNA sequences, and if needed, to optimise primer placement or length by manually editing the primer sequences.

Primer name	Amplicon size	Sequence (5' → 3')
hsp70.3 forward	103bp	AAGCCATCAATACGCCTGAC
hsp70.3 reverse		GCCCAGGTCAATGCCAATAG
hsp70.1/2 forward	191bp	AAAGAGCAGCCTGACAGGAC
hsp70.1/2 reverse		CTGGTCGTTGGCGATGATC
hsf1 forward	158bp	TGATCTCAGATGTCCAGCAC
hsf1 reverse		TGGACCGTGCTAATGTGATC
hsp90aa1.1 forward	180bp	CATTTGGGAATCTGCAGCTG
hsp90aa1.1 reverse		AACCGATGAACTGAGAGTGC
hsp90aa1.2 forward	168bp	ACCCTATCACACTCTTTGTGGAG
hsp90aa1.2 reverse		CGCCATGATCGTGGTCGTC
hsp90ab1 forward	146bp	CTGCTTTCCTCCGGATTCTC
hsp90ab1 reverse		GGAATGTCTTCAGGAGCAGC
hsp90b1 forward	156bp	CTTCCAAGCACAACAACGAC
hsp90b1 reverse		TGGTCTCCAGCTCAAGGTAG
tuba1c forward	193bp	TGCCTCAATCTTGGACAGTG
tuba1c reverse		TGGATGCCATGCTCAAGAC

3.8.2 RNA extraction and quantification

To extract RNA from the samples, the RNeasy^R Mini Kit was used (QIAGEN, 74106). RNAlater was removed from the samples and replaced by 350 μL RLT buffer (40 μL 1M DTT (Invitrogen, Y00147)/1 mL RLT). The tissue was disrupted using a mechanical homogeniser and then centrifuged at max speed (15 000 xg) for 3 min. The supernatant was transferred to new tubes and 350 μL 70% ethanol was added. to precipitate RNA. 700 μL of the samples were added to RNeasy Mini Spin columns (in 2mL collection tubes) and centrifuged at 8000 xg for 15 s. The flow-through was discarded and 700 μL RW1 buffer (supplied) were added before centrifuging at 8000 xg for 15s. 260 ml ethanol were added to the supplied RPE buffer concentrate, and 500 μL added to the columns. After centrifuging at 8000 xg for 15 s, the same volume of RPE was added again, followed by centrifugation for 2 min (8000 xg). To dry the membranes, the columns were placed in new 2mL collection tubes (the flow-through was discarded). They were centrifuged at

15000 xg for 1 min. The columns were placed in new 1.5 mL collection tubes and 30μL RNase-free water was added to elute the RNA. The samples were centrifuged at 8000 xg for 1 min and kept on ice. A Nanodrop spectrophotometer (ThermoFisher, ND-ONE-W) was used to measure the total RNA concentration in each sample. The samples were then standardised to the lowest concentration, and adjusted to a volume of 11 μL for cDNA synthesis.

3.8.3 cDNA synthesis

The lowest RNA concentration was used to normalise all samples by dilution in water in a 96-well PCR plate. Each sample was added 2μL of Mix1 (2.5μM Oligo(dT)20 (Life Technologies corp., 58063) and 0.5mM dNTP mix (Invitrogen, 100004893)). They were heated to 65 °C for 5 min and incubated on ice for at least 1 min. 7 μL of Mix2 (1X First-Strand Buffer (Invitrogen, Y02321), 0.005M DTT (Invitrogen, Y00147), 2U/μL RNaseOut (Invitrogen,100000840) and 10U/μL RT Superscript^{TM} III (Invitrogen, 56575)) were added to each sample and the mixture incubated at 50°C for 30-60 min. The reaction was finally inactivated by heating to 70°C for 15 min.

3.8.4 RT-qPCR

20 μL cDNA synthesis reaction mix (final concentration of 1x iTaq^{TM} Universal SYBR^{R} Green Supermix (BioRad, 1725121), 0.2 μM forward (Sigma-Aldrich), 0.2μM reverse primer (Sigma-Aldrich)) and 5μL of the samples were distributed in the wells of a 96 well hard-shell RT-qPCR plate (BIO Rad, HSP9601). The plate was covered with a transparent Microseal^{R} 'B' seal (BioRad, MSB1001), vortexed, spun down, and run with the RT-qPCR protocol shown below.

Pre-denaturing	95 °C	2 min	
Denaturing	95 °C	15 sec	x37 cycles
Annealing + plate read	60 °C	25 sec	
Extension	95 °C	10 sec	
Final extension	95 °C		
Plate read	5-95 °C		

3.8.5 Primer Efficiency and Specificity

Dilution curves for all primer pairs were made to determine primer efficiencies and the optimal cDNA dilution to use for the RT-qPCR experiments. An efficiency of 80-100% was considered acceptable, as >100% efficiency could be a result of too high Ct value variances between dilutions, while <80% efficiency was considered too low. The best Ct values were chosen to be under 30. Over 30, the number of cycles would be high enough for other sequences to be amplified and give a false positive.
Because a 10-fold dilution series would dilute the samples too much, a 2-fold dilution series was prepared from a cDNA pool, testing the concentrations 1/10, 1/20, 1/40, 1/80, and 1/160 for each of the primer pairs. three technical replicates were run, in addition to a no-template control (NTC)(only nuclease free water) and a no-RT (no enzyme during cDNA synthesis) controls. The NTC control consisted of nuclease free water and was aimed at testing for primer dimer formation or contamination. The no-RT control was aimed at testing for amplification of genomic DNA. Neither of the controls were accepted with a Ct value <34.

The Ct values were plotted against the decreasing logarithmic dilution, and the slope given by the resulting linear trend line was further used to determine efficiency with equations 1 and 2. They were adapted from Pfaffl [59].

$$E = 10^{-(\frac{-1}{slope})} \tag{1}$$

$$\%E = (E - 1) * 100 \tag{2}$$

E = Primer efficiency

The specificity of the primers was tested by analysing the melting curve. If the curve displayed a second peak it was considered to be non-specific of have a high amount of primer-dimer formations (see appendix A.3).

3.8.6 Relative quantification and statistical analysis

RT-qPCR was run on all samples (see appendix A.3, Figures A.4 & A.5) with the optimal cDNA dilution obtained from the dilution curves. The validated primer pairs for the samples and primers for the reference gene were used.

$$R = \frac{(E_{target})^{\Delta Ct_{meantarget}}}{(E_{ref})^{\Delta Ct_{meanref}}} \tag{3}$$

R = Relative expression

E_{target} = Efficiency of gene(s) of interest

E_{ref} = Efficiency of reference gene (*tuba1c*)

$\Delta Ct_{meantarget}$ = the mean Ct value of 2 sample replicates

$\Delta Ct_{meanref}$ = the mean Ct values of 2 sample replicates of reference gene (*tuba1c*)

The statistical analysis to determine the significance of the different mRNA levels was performed in RStudio. Normality of the data was tested with the Shapiro-Wilk normality test (p-value<0.05). Statistical significance was determined using the Student's t-test (p-value<0.05). The data were plotted in boxplots made with the same software.

3.9 Western Blot on heat shocked Zebrafish Larvae (5dpf)

We wanted to investigate the levels of HSR-related proteins during the recovery period following heat shock. Western blot was therefore performed on protein extracts from 5 day-old zebrafish larvae, both with and without the heat shock treatment.

3.9.1 Protein Extraction and Quantification

Sampling was done as described in the HS section. The samples were suspended in 150 μL Lysis Buffer (1X RIPA Lysis Buffer (20-188, EMD Milipore) and cOmplete^{TM} Mini Protease inhibitor Cocktail (04693124001, Sigma)) and mechanically homogenised with a pellet mixer and incubated on an orbital shaker at 11°C o/n. To increase lysis, the samples were again homogenised after the incubation period. They were centrifuged 20 min at 12000 rpm at 4°C. The supernatant was transferred to new tubes.

The BCA Protein Assay kit (Scientific Fisher, no.23225) was used to measure total protein concentration in the samples. 10μL of the samples were distributed in triplicates

in a 96 well Costar plate (CLS9017, Sigma Aldrich). The supplied BSA standards were diluted with nuclease-free water to have concentrations of 0μg/μL, 5μg/μL, 10μg/μL, and 20μg/μL. They were distributed in triplicates in the microplate, and 100 μL of the supplied working reagent (1/50 reagent B, 49/50 reagent A) were added to each well. The plate was covered with parafilm, and mixed for 30 seconds on a plate shaker. The plate was incubated at 37 °C for 29.5 min, before cooling at RT for 3 min. Using a Spark^R Microplate Reader (TECAN), the plate was read at a wavelength of 562nm. The samples were then normalised to the lowest concentration measured (1.89μg/μL) with RIPA-i buffer, and 15 μL were distributed in PCR tubes.

3.9.2 SDS page

2X Laemmli buffer (80% Laemmli 2X (BioRad, 1610737)+ 20% 1M DTT (Sigma, 43816-10ML)) was prepared. 15μL of the buffer were added to each sample. To be able to visualise the standards without on the PAGE gel and membrane at all stages, 0.35μL 1/60 diluted Unstained standards (BioRad, 1610363) were mixed with 5μL All Blue standards (BioRad, 1610373). The solutions were denatured for 4' at 90°C. Pre-cast Criterion TGX Stain-free PAGE gels (BioRad, 567-8094) were prepared by removing the comb and the bottom tape. They were placed in the chamber in 1X TGS buffer (1610732, Invitrogen) in both the outside and in the gel chamber. The samples and ladder were loaded and the gels were run for 45 min at 150V. The plastic cases were carefully cracked open and the gel was imaged in a ChemiDoc^{TM}Touch after activation by exposure to UV-light for 45sec to visualise total protein amount. The gel was then transferred to a PVDF membrane (Trans-Blot^R Turbo^{TM} Midi PVDF Membrane Transfer Pack (BioRad, 170-4157) by layering in the following order: bottom wet pad, PVDF membrane, the gel, and top wet pad. To transfer the proteins from the gel to the membrane (blotting), the cassette was run for 30 min at 80V. After the blotting the membrane was rinsed in 1X TBS (50mM Trizma HCl (Sigma, T3253), 150 mM sodium choloride (Sigma, S7653)) + 0.1% Tween20 (Sigma, P9416) (TBS-T).

3.9.3 Immunodetection

To block unoccupied sites on the proteins the membranes were incubated in TBS-T-Cas blocking buffer (1X TBS + 0.1% Tween20 + 1X Casein) for 1 hour. The buffer was then

replaced by the primary antibody solution (Rb α-Hsp70 1:1000 (PA5-72281, Invitrogen) in TBS-T-Cas). They were incubated on an orbital shaker at 11°C o/n. To remove all antibody solution the membranes were first flushed and then washed 3 x 5 min in TBS-T on an orbital shaker in RT. Incubation in secondary antibody solution (Strep-HRP 1:20 000 (BioRad, 160381) + α - Rb-HRP 1:20 000 (BioRad, A16023)) followed for 1h in RT, where Strep-HRP is used to detect the standards. The washing steps with TBS-T were then repeated. For the immunodetection, the ECL buffer was prepared (50% clarity Luminol Substrate + 50% Clarity Peroxide Solution (BIO RAD, 1705060)). The membrane was dipped in ECL buffer for 30sec and transferred into a plastic sleeve and onto the ChemiDoc tray. The Chemiluminescence function was used for imaging at different exposures ranging from 6-120sec.

3.9.4 Protein quantification and statistical analysis

To quantify the amount of protein in the samples, an image of the activated SDS-PAGE gel was used as reference. The mean grey value of a band that was present in all lanes was measured using ImageJ. The same was done with a picture of the PVDF membrane. The ratio between the average sample and the average reference mean grey area was calculated, and the results plotted and statistically analysed using RStudio.

Machines

Machine	**Manufacturer**
Centrifuge 5424R	Eppendorf
GeneAmp^{R} PCR System 2700	Applied Biosystems (AB)
G:BOX GelDoc	SYNGENE
Leica Research Cryostat CM3050-S	Leica
Leica DM LS Microscope	Leica
Slide scanner Axio Scan Z1	Zeiss
Confocal Microscope FV3000	Olympus
Nanodrop spectrophotometer ND-ONE-W	ThermoFisher
CFX96^{TM} Real-Time PCR detection system	BioRad
Spark^{R} Microplate Reader	TECAN
ChemiDoc^{TM}Touch Imaging System	BioRad
Trans-blot^{R} Turbo^{TM}	BioRad

Equipment

Equipment	**Catalogue Number**	**Manufacturer**
Superfrost^{TM}Plus Adhesion Microscope Slides	J1800AMNZ	Epredia
Menzel-Gläser	#1,5	
RT-qPCR hard-shell plate	HSP9601	BioRad
Microseal^{R} 'B' seal Seals	MSB1001	BioRad
Costar plates	CLS9017	Sigma Aldrich
Pre-cast Criterion TGX Stain-free PAGE gel	567-8094	BioRad
Trans-blot^{R} Turbo^{TM} Midi PVDF Membrane - Transfer Pack	170-4157	BioRad

Reagents

Reagent	**Catalogue Number**	**Manufacturer**
Proteinase K	1114885	QIAGEN
Nuclease free water	R0582	Thermo Fisher Scientific
10X Taq Reaction Buffer	B9014S	NEB
10mM dNTP Mix	N0447S	NEB
Taq DNA Polymerase	FB-6000-50	Fisher BioReagents
PCR primers	-	Sigma
10X Cutsmart Buffer	B7206S	NEB
Mlu1-HF Restriction Enzyme	R3198L	NEB
1X TAE Buffer	50004	SeaKem
Agarose	A9539	Sigma-Aldrich
Gelred	41003	Biotium
6x Loading Dye	R0661	Thermo Fisher Scientific
GeneRuler 100 bp DNA Ladder	SM0331	Thermo Fisher Scientific
Paraformaldehyde (PF)	15714-S	Chemi-Teknik as
PBS	524650-1EA	EMD Milipore
NucBlue mounting medium	P36981	Thermo Fisher Scientific
OCT Medium	4583	Sakura
Triton^{TM} X-100	T8787	Sigma
MS X Parvalbumin	MAB1572	EMD Milipore
Goat MS X AlexaFluor555	A32727	Thermo Fisher Scientific
Casein Blocking Buffer 10X	B6429	SIGMA
RNALater	MKCH4082	Sigma
RNeasy^{R} Mini Kit	74106	QIAGEN
Oligo(dT)20	58063	Life Technologies corp.

1X First Strand Buffer	Y02321	Invitrogen
DTT	Y00147	Invitrogen
10mM dNTP MIX	100004893	Invitrogen
RNaseOut	100000840	Invitrogen
RT Superscript ^{TM} III	56575	Invitrogen
iTaq Universal SYBR^{R} Green Supermix	1725121	BioRad
RT-qPCR primers	-	Sigma-Aldrich
RIPA Lysis Buffer 10X	20-188	EMD Milipore
cOmplete^{TM} Mini Protease Inhibitor Cocktail	04693124001	Sigma
BCA Protein Assay kit	no.23225	Thermo Fisher Scientific
2X Laemmli buffer	1610737	BioRad
DTT	43816-10ML	SIGMA
Unstained Standards	1610363	BioRad
All Blue Standards	1610373	BioRad
10X TGS	1610732	BioRad
Trizma HCl	T3253	Sigma
Sodium Chloride	S7653	Sigma
Tween 20	P9416	Sigma
Rb α-Hsp70	PA5-72281	Invitrogen
Precision Protein^{TM} StrepTactin-HRP Conjugate	1610381	BioRad
α - Rb-HRP 1:20 000	A16023	Thermo Fisher Scientific
Clarity Luminol Substrate + Clarity Peroxide Solution	1705060	BioRad

Software and webpages

Software	**Version**	**Link**
ImageJ	1.8.0_172	https://imagej.nih.gov/ij/download.html
Photoshop	23.2.2.	https://www.adobe.com/no/products/photoshop.html
Neutube	1.0z	https://neutracing.com/
Zen Blue Edition	3.5.093.00000	https://www.zeiss.com/microscopy/us/products/microscope-software/zen-lite.html
RStudio	2021.09.1+372	https://www.rstudio.com/products/rstudio/download/#download
Seaview	5.0.5	http://doua.prabi.fr/software/seaview
Ensembl	106	https://www.Ensembl.org
Primer3	4.1.0	https://Primer3.ut.ee
Oligocalc	3.27	http://biotools.nubic.northwestern.edu/OligoCalc.html

4 Results

4.1 Genotyping of fish

To identify and study the UBOX-/- zebrafish we genotyped adult fish by restriction enzyme analysis. The target sequence of the Mlu1 restriction enzyme was destroyed by the CRISPR-Cas deletion in exon 8 of *stub1* (Figure 1.6). We were thereby able to identify homozygous and heterozygous mutants and wild type fish using the location of the restriction site to predict DNA fragment sizes. Wild-type fish showed two bands at 54bp and 173bp, while homozygous mutants showed one band at 246bp (Figure 3.1). The heterozygous fish showed all three band sizes (54bp, 173bp and 246bp).

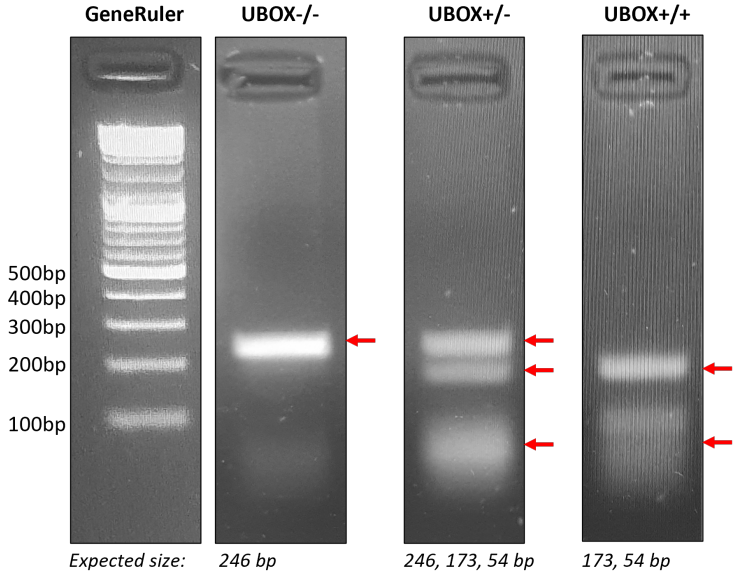

Figure 4.1: ***Genotyping of U-box mutant zebrafish.*** *2.5% Agarose gel with a 100bp GeneRuler used as DNA ladder (left lane). The PCR product amplified from genomic zebrafish DNA was cut with the Mlu1 restriction enzyme and run on the gel. Large DNA fragments (246bp) were present in both the homozygous (UBOX-/-) and heterozygous (UBOX+/-) mutant. 173 bp fragments were seen in the heterozygous mutant and the wild-type (UBOX+/+), as well as faint bands at 54bp.*

4.2 Investigating signs of neurodegeneration in 3 year old zebrafish

We started by testing both custom made and commercial Chip antibodies for IHC. None of these were considered to be specific to Chip (data not shown). Further, three Heat Induced Epitope Retrieval (HIER) methods were tested to try and increase specificity, nei-

ther of which improved the result (not shown)[60][61]. Western blot was then performed with the same antibodies to evaluate if they could be used for Chip protein quantification. This also resulted in non-specific bands at different sizes than the expected size of 37kDa (data not shown). Staining the brain sections for parvalbumin, which has been shown to be localised in zebrafish Purkinje cells [53] facilitated instead visualisation of Purkinje cells and their dendrites, which extend from the PCL into the molecular layer of the cerebellum (ML). The cell bodies can be seen in the PCL, and their axons branch and extend into the granular cell layer (GCL)(Figure 4.2*b, c*). A general overview of the zebrafish brain is shown in Figure 4.2a: an illustration (A), the wild-type (B) and mutant (C) IHC stained brain sections. Parvalbumin was localised in the cerebellum, while NucBlue stained nuclei in the ML and LCa. Figure 4.2b shows the cerebellum while 4.2c shows the posterior region of the cerebellum for a closer look at dendrite structure.

To investigate if the cerebellum size in the mutant differed from the wild-type, we measured areas in the zebrafish brain (see Figure 3.2). We then calculated the ratios between the ML and the cerebellum diameter (Figure 4.3a) and between the cerebellum diameter and cerebellum + TeO diameter (Figure 4.3b).

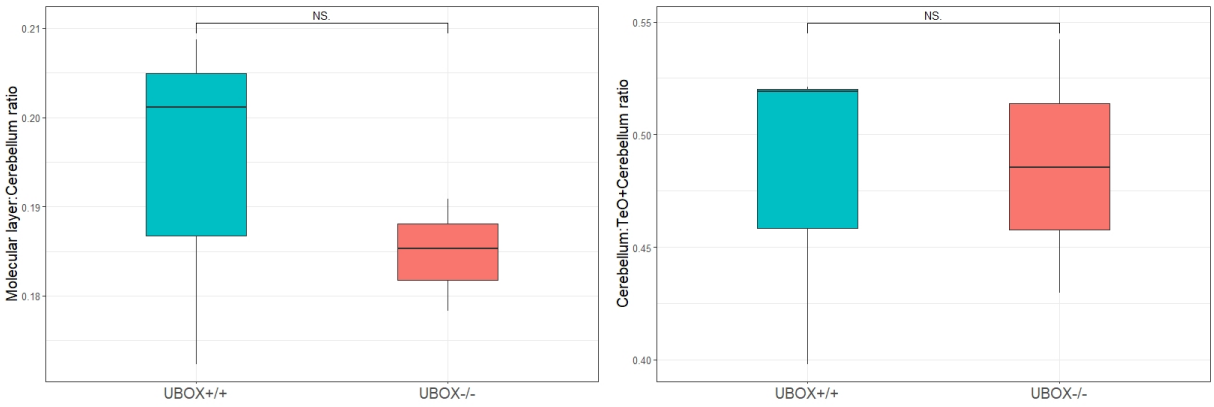

(a) ***ML size relative to cerebellum size.*** **(b)** ***Cerebellum size relative to cerebellum + TeO size.***

Figure 4.3: ***Measurements of zebrafish cerebellum and ML sizes.*** *Statistical method: Student's t-test, where $p<0.05$. NS.=not significant. n=3*

There was no significant decrease in ML size compared to cerebellum size in the mutant, though a decreasing trend could be observed (Figure 4.3a). The cerebellum size relative to the size of the brain did not vary between the two genotypes (Figure 4.3b).

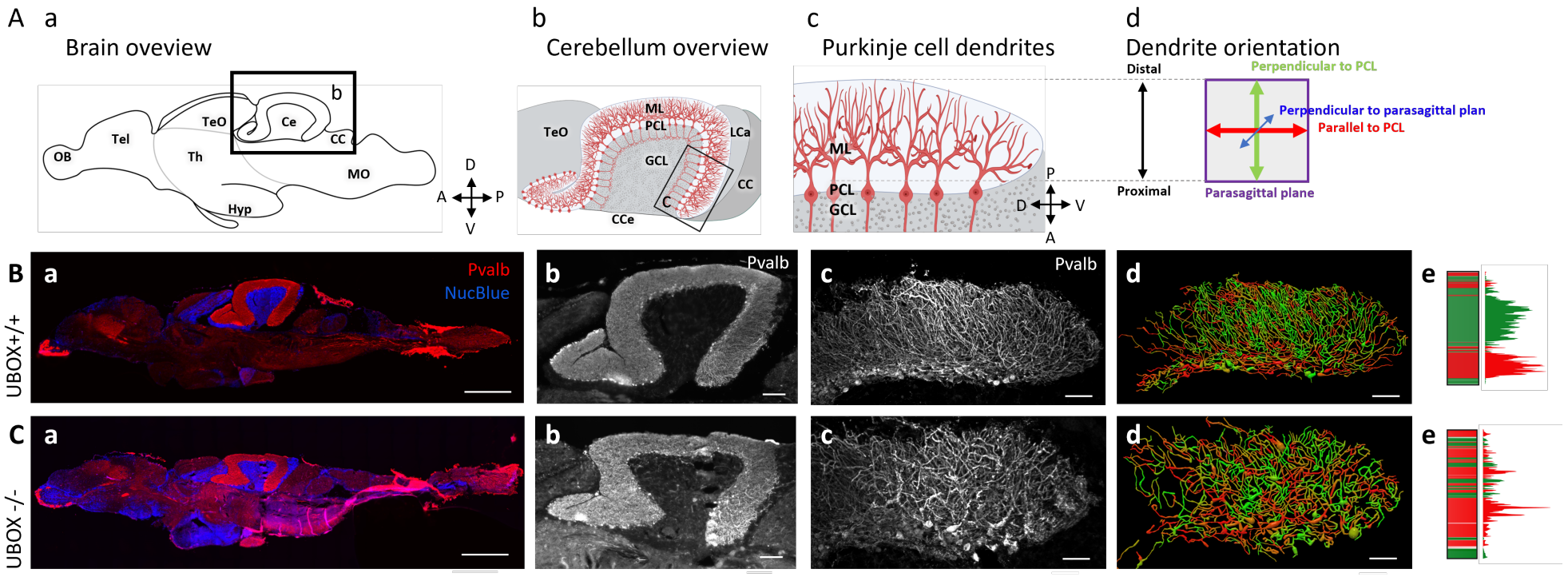

Figure 4.2: *Visualisation of zebrafish brain and cerebellum with Pvalb staining.*[1]

4.2.1 Purkinje cell amount in the cerebellum

Previous studies have shown that neurodegeneration by the absence or dysfunction of Chip leads to cerebellar degradation. In particular, a decrease in Purkinje cell body number has been recorded [51]. We therefore analysed the number of Purkinje cell bodies in UBOX-/- and UBOX+/+ zebrafish (Figure 4.4a).

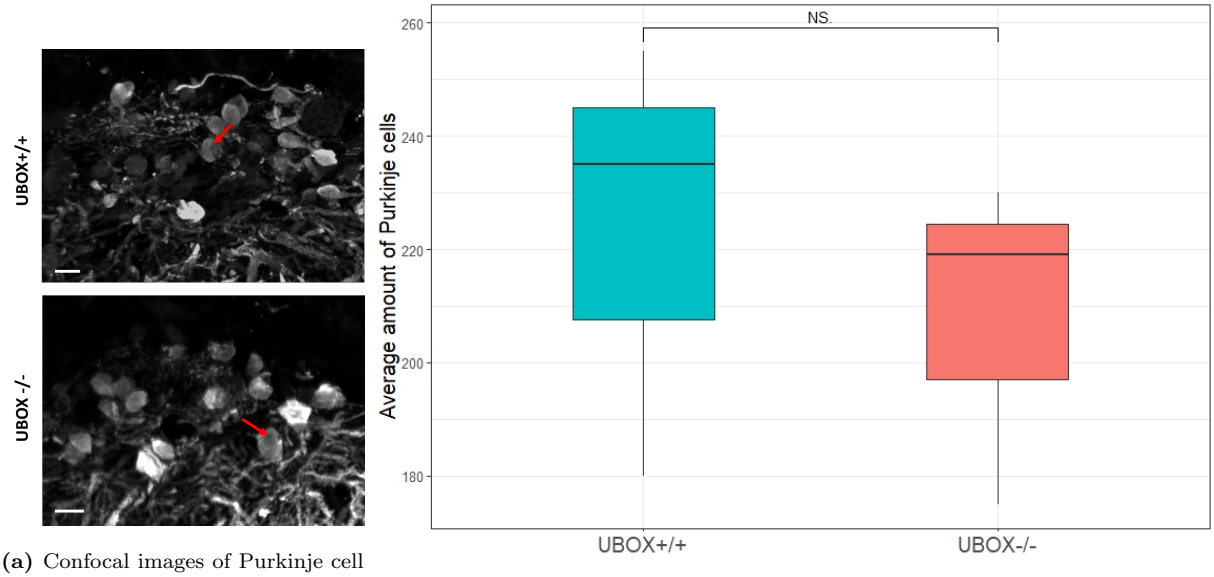

(a) Confocal images of Purkinje cell bodies.

(b) Boxplot of Purkinje cell body amount.

Figure 4.4: ***Number of Purkinje cells present in the PCL of the cerebellum.*** *The Purkinje cell bodies located in the PCL (red arrows, a) were counted on three brain sections per individual (b). Scale bars: 10µm. Statistical analysis revealed no significant change in cell body number between UBOX-/- and UBOX+/+ samples. Statistical method: Student's t-test, where p<0.05. NS.=not significant. n=3.*

We could not see a significant difference in Purkinje cell body numbers (Figure 4.4b), however there was a trend indicating fewer cell bodies in the mutant compared to the wild-type.

[1] ***Figure 4.2: Visualisation of zebrafish brain and cerebellum with Pvalb staining.*** *The posterior regions of the cerebellum in the wild-type (A) and homozygous mutant (B). Illustrations of the whole brain (a), OB: olfactory bulb, Tel: telencephalon, TeO: tectum opticum, Ce: cerebellum, CC: crista cerebellaris, Th: thalamus, MO: medulla oblongata, Hyp: hypothalamus. The cerebellum (b), LCa: lobus caudalis cerebelli , CCe: corpus cerebellaris, and posterior cerebellum region (c). The orientation relative to the parasagittal plane can be seen in (d). Whole brain scans stained with NucBlue (blue) and Pvalb (red) can be seen in a. Greyscale image of the cerebellum pvalb staining and posterior region of the cerebellum are shown in b and c, respectively. The neurotracing projections (d) were obtained from NeuTube. The visualisation of dendrites predominantly parallel (red) or perpendicular (green) to PCL can be seen in e. Scale bars= a:500µm, b: 200µm, c&d: 50µm.*

4.2.2 Dendrite orientation

To further investigate the morphological consequences of the dysfunction of Chip's U-box domain, we studied Purkinje cell dendrite orientation in the posterior region of the cerebellum. Three wild-type and three mutants were analysed (see appendix A.2), one of each is presented in Figure 4.2.

The neurotracing reconstruction showed that the dendrite orientation in wild-type (UBOX+/+) samples is predominantly parallel to the PCL (red in 4.2Ad) when looking at the area most proximal to the PCL. When looking at the distal part of the ML, the dendrites migrate more perpendicular to the PCL (green in 4.2Ad). The dendrites in the mutant (UBOX-/-)(4.2Bc & 4.2Bd) seem to grow less structured, with areas close to the PCL where dendrites grow both parallel (red in 4.2Bd) and perpendicular (green in 4.2Bd) to the PCL. In the distal half, there seem to be more dendrites growing predominantly parallel to the PCL (red). Quantification of the neurotracing reconstructions is shown in Figure 4.2e and Figure 4.5.

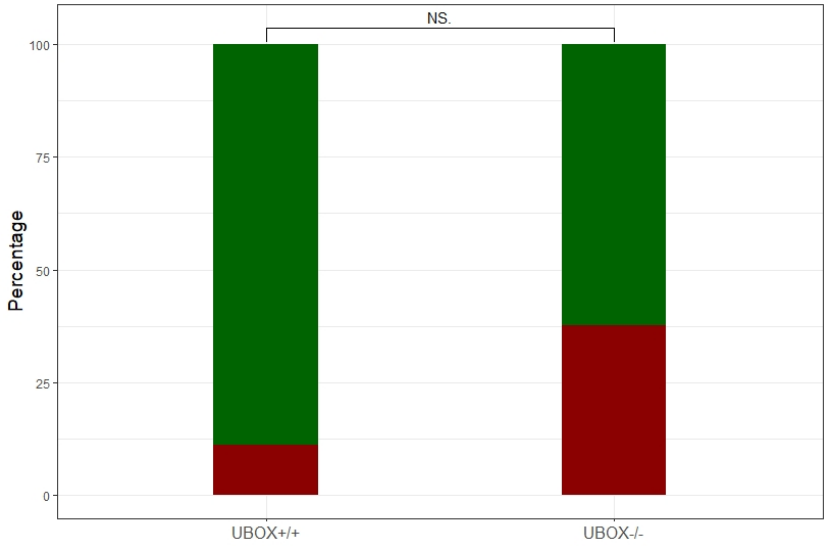

Figure 4.5: ***Quantification of dendrite orientation.*** *Green shows amount of pixel rows where dendrites grew predominantly perpendicular to PCL, while red shows amount of areas where dendrites grew predominantly parallel to PCL. Results were obtained using Neutube to make neurotracing reconstruction and using ImageJ ans Photoshop to measure colour dominance. Statistical method: Student's t.test, where $p<0.05$. NS.=not significant. n=3.*

Plotting the quantification results revealed a not statistically significant difference between the wild-type and the mutant samples, though a trend could be observed (Figure 4.5). More dendrites extended predominantly parallel to the PCL in the mutant than in

the wild-type (red area), while less extended predominantly perpendicular to the PCL in the mutant than in the wild-type (green area).

4.3 Heat Shock

It has been shown that some NDs such as SCAR16 are induced early in life, and increase the cells sensitivity to environmental stress. We therefore chose to expose zebrafish larvae to stress to monitor survival and hatching patterns. Heat stress is known to disturb homeostasis and induce the HSR as a protective mechanism. Larvae were exposed to heat at 24hpf and were observed up to 5 dpf. They showed no death or change in hatching pattern (data not shown). Therefore the focus was directed towards changes in the HSR on a molecular level, investigating activation and recovery at the mRNA level (RT-qPCR) and the protein level (Western blot).

4.3.1 Transcript levels of *hsf1*, *hsp70*, *hsp90* following heat-shock

The efficiency of the custom made RT-qPCR primers was tested by running a two-fold dilution series, and the results were plotted (Figure 4.6) and analysed (Table 1). Four primer pairs had to be designed for the *hsp90* paralogues and two for the *hsp70* paralogues, where the same pair was used for *hsp70.1* and *hsp70.2*. One primer pair was sufficient for *hsf1*. *Tuba1c* primers were used for normalisation.

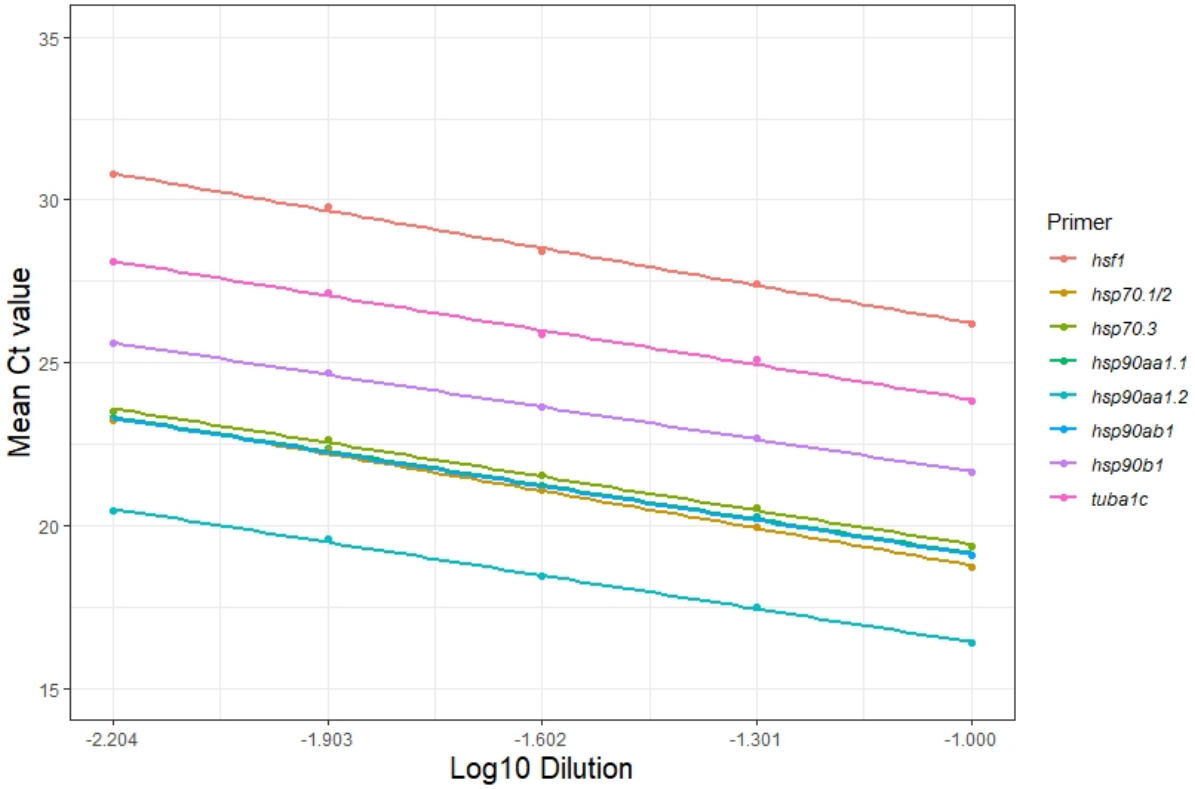

Figure 4.6: ***Dilution curves for hsp70, hsp90, hsf1, and tuba1c primers.*** *Zebrafish RNA extract was used to test primers on a two-fold dilution series of 1:10, 1:20, 1:40, 1:80, and 1:160. The logarithm of the dilution (x-axis) was plotted against the mean Ct value (y-axis). Linear regression was performed to obtain the regression line and function (values shown in table 1).*

Table 1: ***Values obtained from dilution curves for RT-qPCR primers.*** *The primers for the listed genes were tested on a two-fold dilution series. The regression line equation yielded slope, intercept and R^2, which were used to calculate the primer efficiencies.*

Primer pair	Slope	Intercept	Efficiency (E)	Efficiency (%)	R^2
hsf1	-3.8206	22.403	1.827	82.70	0.9978
hsp70.1/hsp70.2	-3.7877	14.992	1.837	83.66	0.9984
hsp70.3	-3.4618	15.958	1.945	94.48	0.9973
hsp90aa1.1	-3.4751	15.679	1.94	93.98	0.9987
hsp90aa1.2	-3.3987	13.019	1.969	96.89	0.9989
hsp90ab1	-3.4784	15.626	1.939	93.86	0.9993
hsp90b1	-3.2975	18.362	2.01	101.03	0.9993
tuba1c	-3.5282	20.348	1.921	92.06	0.9950

The primer efficiencies (Table1) were all found to be within the accepted range of 80-120%. Primers for *hsf1* and *hsp70.1/hsp70.2* had the lowest efficiencies (just over 80%), while the *hsp90b1* primers showed an efficiency of 101%. The R^2 values were close to 1 (between 0.9950 and 0.9993), indicating a linear regression line and hence linearity of the amplification. The slope of most of the primer pairs was close to -3.3, indicating 3.3 amplification cycles between each dilution. This corresponds to an efficiency of >90%. Two pairs had an efficiency of 82-83%, even after optimisation (increasing temperature from 60°C to 62°C during annealing in the RT-qPCR cycle). The NTC consisting of nuclease-free water gave no results for all primers, indicating that there was no contamination of the samples. The no-RT control, containing RNA instead of cDNA, gave either no results, or amplification only after cycle 31. The melting curves (see appendix A.3) showed one single peak for almost all primer pairs, indicating that there were no primer-dimer formations or unspecific amplification of genomic DNA. For *hsp90b1* there was a second peak, but the no-RT showed un-specific amplification only after 31 cycles, 6 cycles later than the amplification at the highest dilution of 1:160 (25 cycles), and 10 cycles later than the dilution we further used (1:10, 21 cycles). The standard deviation between all technical triplicates for the 1:10 dilution was lower than 0.3 for all primer pairs.

The RT-qPCR results presented beneath will not address the differences between the non-heat-shocked samples, as they were all relatively low and displayed not significant changes. They were included as negative controls to compare to the heat-shocked samples.

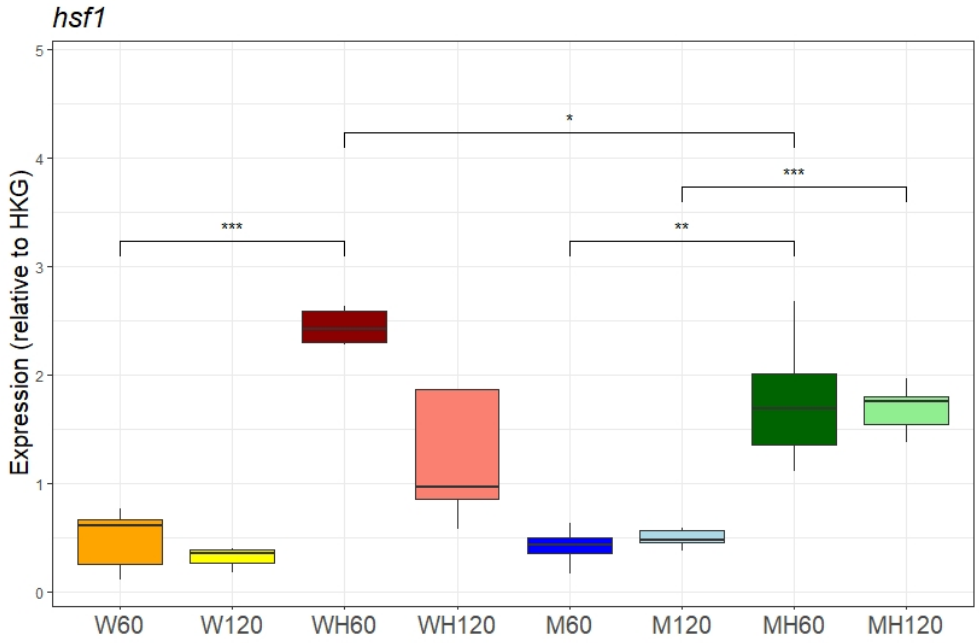

Figure 4.7: ***Box plot of relative hsf1 expression in 5dpf old larvae after 60 min heat shock recovery period.*** *Wild-type larvae (W) and homozygous mutant larvae (M) were exposed to 60 min heat shock at 38°C (WH & MH). RNA was extracted after two different recovery period durations (60 & 120 min). Expression on the y-axis was normalised to the HKG (tuba1c). Statistical method: Student's t-test, statistical significance indicated with asterisks (*p<0.05, **p<0.01, ***p<0.001). W60: n=3, WH120: n=5, others: n=6.*

RT-qPCR revealed significant increase in *hsf1* transcript levels in the heat-shocked wild-type at 60 min compared to the non-heat-shocked wild-type (Figure 4.7). The same was seen for the mutant at both time points. No significant change could be seen in transcript levels comparing 60 min and 120 min recovery. There was a significant decrease in the heat-shocked mutant (MH) at 60 min recovery compared to the wild-type (WH).

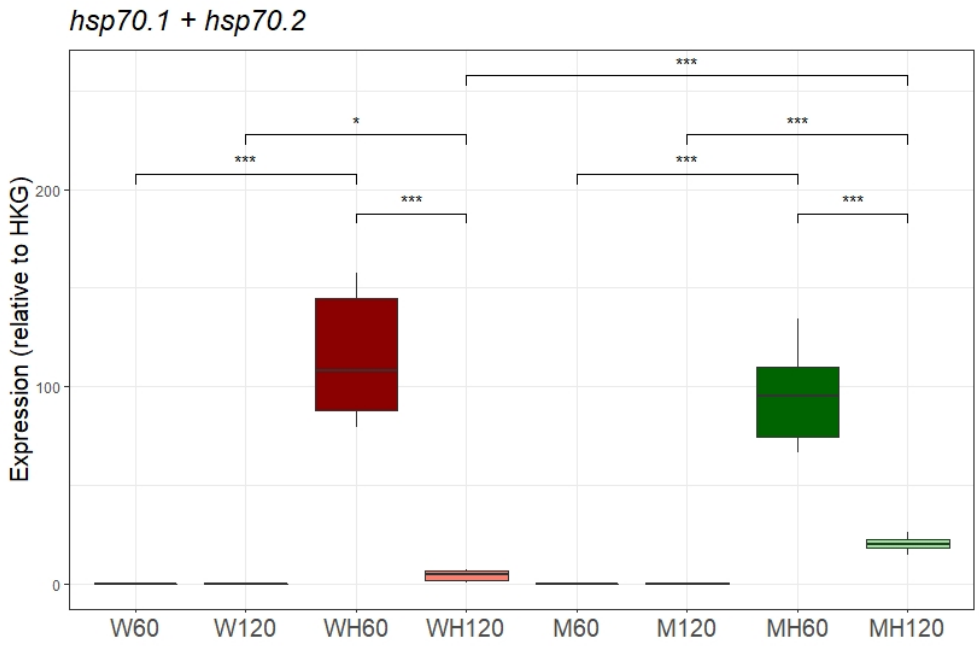

Figure 4.8: ***Box plot of relative hsp70.1 and hsp70.2 expression in 5dpf old larvae after 60 min heat shock recovery period.*** *Wild-type larvae (W) and homozygous mutant larvae (M) were exposed to 60 min heat shock at 38° C (WH & MH). RNA was extracted after two different recovery period durations (60 & 120 min). Expression on the y-axis was normalised to the HKG (tuba1c). Statistical method: Student's t-test, statistical significance indicated with asterisks (*p<0.05, ***p<0.001). W60: n=3, WH120: n=5, others: n=6.*

For *hsp70.1* and *hsp70.2* there was an increase in transcript levels after heat shock in the wild-type (W), and a significant decrease from 60 to 120 min recovery (Figure 4.8). For the mutant (M), there was a significant increase after heat shock at both time points. There was a significant decrease in the heat-shocked mutant (MH) from 60 to 120 min recovery. However, after 120 min recovery there was a significantly higher level of transcript in the heat-shocked mutant than in the heat-shocked wild-type.

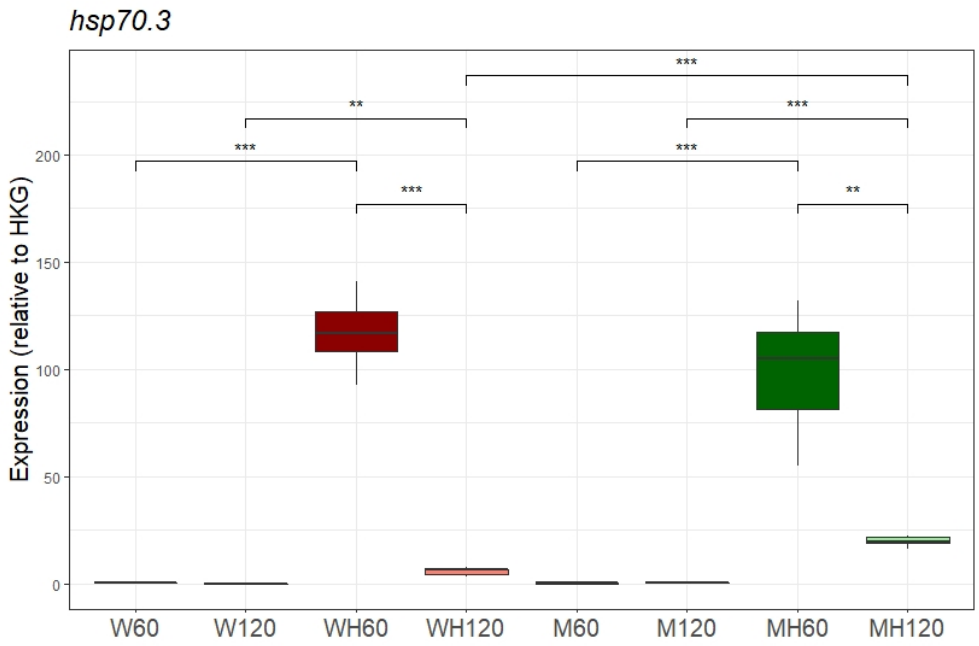

Figure 4.9: ***Box plot of relative hsp70.3 expression in 5dpf old larvae after 60 min heat shock recovery period.*** *Hsp70.1 and Wild-type larvae (W) and homozygous mutant larvae (M) were exposed to 60 min heat shock at 38° C (WH & MH). RNA was extracted after two different recovery period durations (60 & 120 min). Expression on the y-axis was normalised to the HKG (tuba1c). Statistical method: Student's t-test, statistical significance indicated with asterisks (**p<0.01, ***p<0.001). W60: n=3, WH120: n=5, others: n=6.*

RT-qPCR showed a higher transcript level of *hsp70.3* after heat shock in the wild-type (W). A significant decrease of transcript level from 60 to 120 min could be seen in the heat-shocked wild-type (Figure 4.9). For the mutant (M), there was a significant increase with heat shock at both time points. There was a significant decrease in the heat-shocked mutant from 60 to 120 min recovery. However, similar to *hsp70.1/2*, there was a significantly higher level of transcript in the mutant after 120 min than in the wild-type after 120 min recovery.

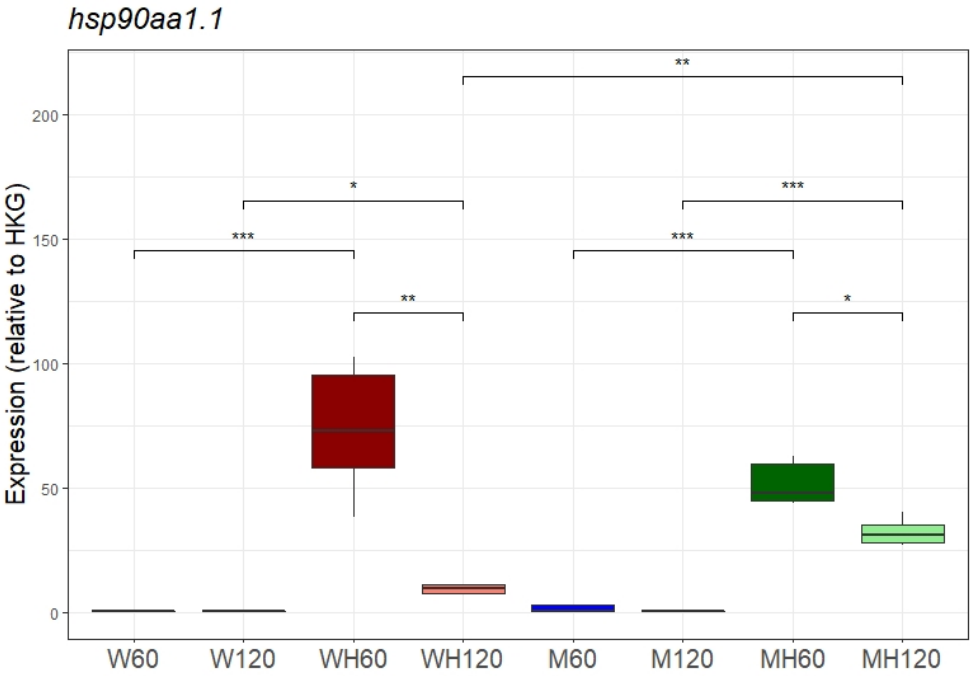

Figure 4.10: ***Box plot of relative hsp90aa1.1 expression in 5dpf old larvae after 60 min heat shock recovery period.*** *Wild-type larvae (W) and homozygous mutant larvae (M) were exposed to 60 min heat shock at 38°C (WH & MH). RNA was extracted after two different recovery period durations (60 & 120 min). Expression on the y-axis was normalised to the HKG (tuba1c). Statistical method: Statistical method: Student's t-test, statistical significance indicated with asterisks (*p<0.05, **p<0.01, ***p<0.001). W60: n=3, WH120: n=5, others: n=6.*

Hsp90aa1.1 results revealed a higher transcript level after heat-shock in the wild-type (WH) after both 60 min and 120 min recovery (Figure 4.10). A significant decrease was also observed from 60 min to 120 min recovery in the heat-shocked wild-type. The same trends are present in the mutant samples (MH). In addition, as was also shown for *hsp70*, a higher level of transcripts was present in the heat-shocked mutant at 120 min recovery compared to the wild-type.

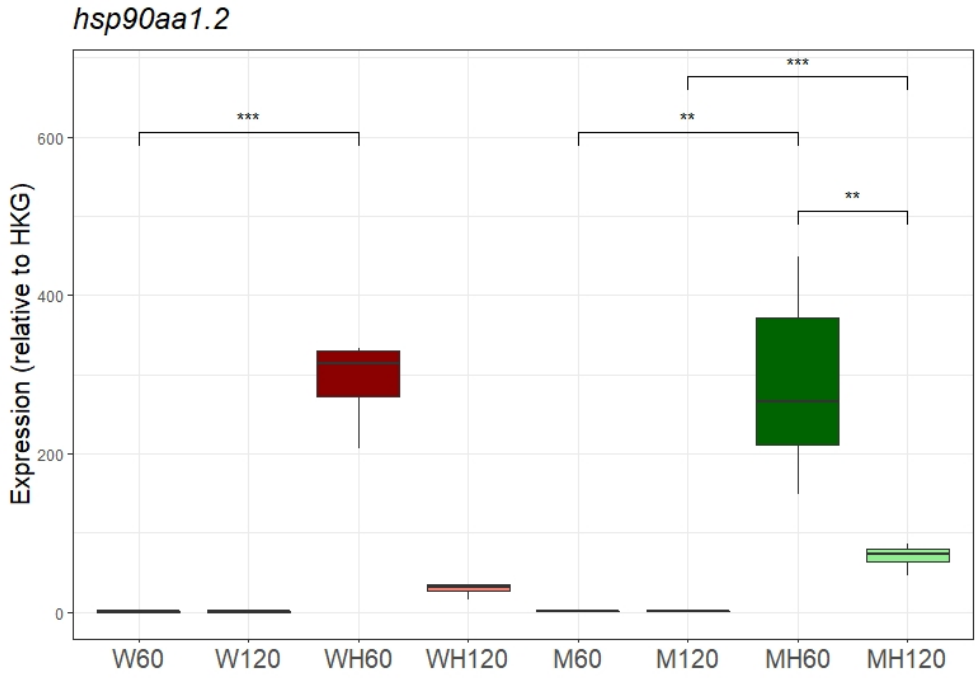

Figure 4.11: ***Box plot of relative hsp90aa1.2 expression in 5dpf old larvae after 60 min heat shock recovery period.*** *Wild-type larvae (W) and homozygous mutant larvae (M) were exposed to 60 min heat shock at 38°C (WH & MH). RNA was extracted after two different recovery period durations (60 & 120 min). Expression on the y-axis was normalised to the HKG (tuba1c). Statistical method: Student's t-test, statistical significance indicated with asterisks (**p<0.01, ***p<0.001). W60: n=3, WH120: n=5, others: n=6.*

Hsp90aa1.2, which has the highest transcript levels of all four *hsp90* paralogues, showed the same trend as was seen in *hsp70/90* and *hsf1* before; an increase in transcript levels after heat-shock compared to no heat-shock in the wild-type (W) at 60 min recovery, though not 120 min (Figure 4.11). Contradictory to *hsp90aa1.1*, *hsp90aa1.2* displayed no statistically significant difference in transcript levels between 60 min and 120 min recovery in the heat-shocked wild-type, though a negative trend could be seen. The mutant (M) had an increase in the heat-shocked samples compared to non-heat-shocked, and a decrease at 120 min compared to 60 min recovery in both heat-shocked samples.

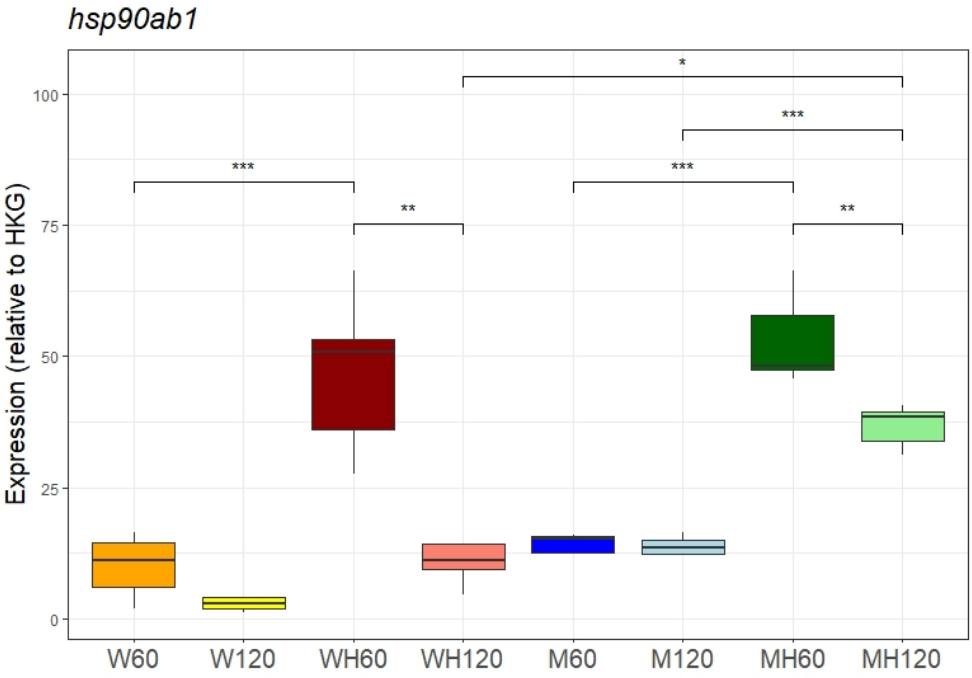

Figure 4.12: ***Box plot of relative hsp90ab1 expression in 5dpf old larvae after 60 min heat shock recovery period.*** *Wild-type larvae (W) and homozygous mutant larvae (M) were exposed to 60 min heat shock at 38°C (WH & MH). RNA was extracted after two different recovery period durations (60 & 120 min). Expression on the y-axis was normalised to the HKG (tuba1c). Statistical method: Student's t-test, statistical significance indicated with asterisks (*p<0.05, **p<0.01, ***p<0.001). W60: n=3, WH120: n=5, others: n=6.*

Hsp90ab1 results revealed the same trend as for all the other genes; a significant increase in transcript levels after heat-shock in the wild-type (W) at 60 min recovery, though not at 120 min (Figure 4.12). A significant decrease was seen from 60 min to 120 min recovery. The increase in transcript levels from the heat-shock was also seen in the mutant (M). In addition, as was also shown for *hsp70*, a higher level of transcripts was present in the heat-shocked mutant at 120 min recovery compared to the wild-type.

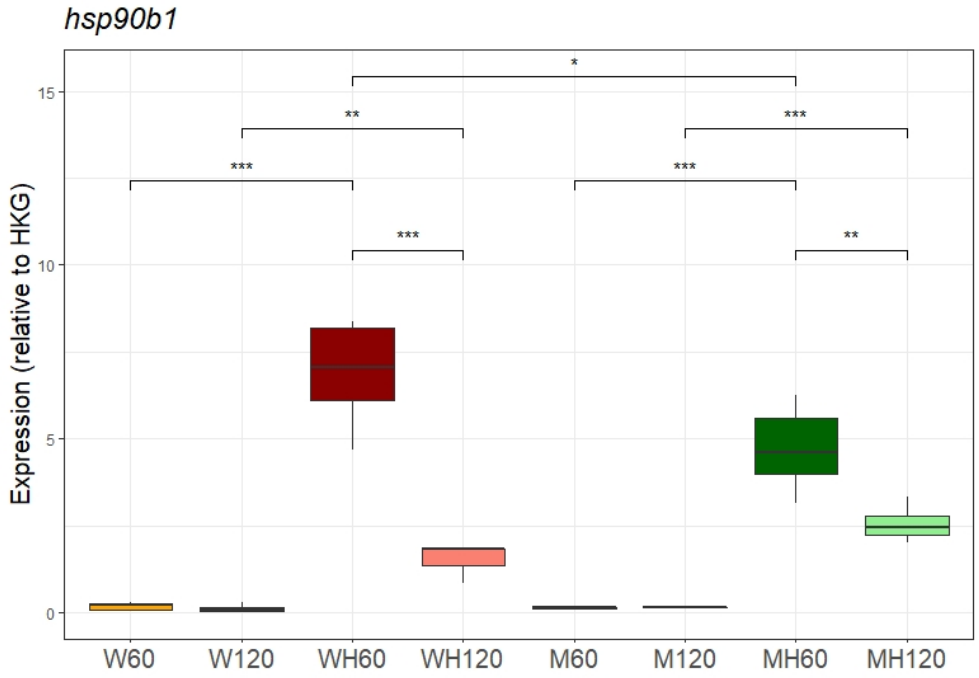

Figure 4.13: ***Box plot of relative hsp90b1 expression in 5dpf old larvae after 60 min heat shock recovery period.*** *Wild-type larvae (W) and homozygous mutant larvae (M) were exposed to 60 min heat shock at 38°C (WH & MH). RNA was extracted after two different recovery period durations (60 & 120 min). Expression on the y-axis was normalised to the HKG (tuba1c). Statistical method: Student's t-test, statistical significance indicated with asterisks (*p<0.05, **p<0.01, ***p<0.001). W60: n=3, WH120: n=5, others: n=6.*

Hsp90b1 showed the lowest relative expression of all *hsp90* paralogues. As for all other genes, an increase of transcript levels after heat-shock was observed (Figure 4.13). In the wild-type, only the heat-shocked samples showed a significant decrease from 60 min to 120 min recovery. The same trends were seen for the mutant (M). There was also a higher transcript amount in the heat-shocked mutant than in the heat-shocked wild-type at 60 min.

To conclude, all *hsp*s showed the same general trends in RNA levels before and after heat shock and approximately the same level of induction of the HSR in both genotypes. A significant delay of HSR termination in the mutant could also be seen for *hsp70* and *hsp90aa1.1* (at 120 min recovery). For *hsf1* there was an increase in transcript after heat-shock (except for the heat-shocked wild-type at 120 min), and a significant increase in the heat-shocked mutant at 60 min compared to the wild-type.

4.3.2 Protein levels of Hsp70 during heat-shock recovery

Analysing the transcript levels of the proteins involved in the HSR gives us an idea of transcriptional regulations. To complement this information and understand the transcription-translation relations, the protein levels of Hsp70 were measured. Western blot was performed on protein extracts from 5dpf larvae exposed to 60 min heat shock and sampled after a 60 min recovery period.

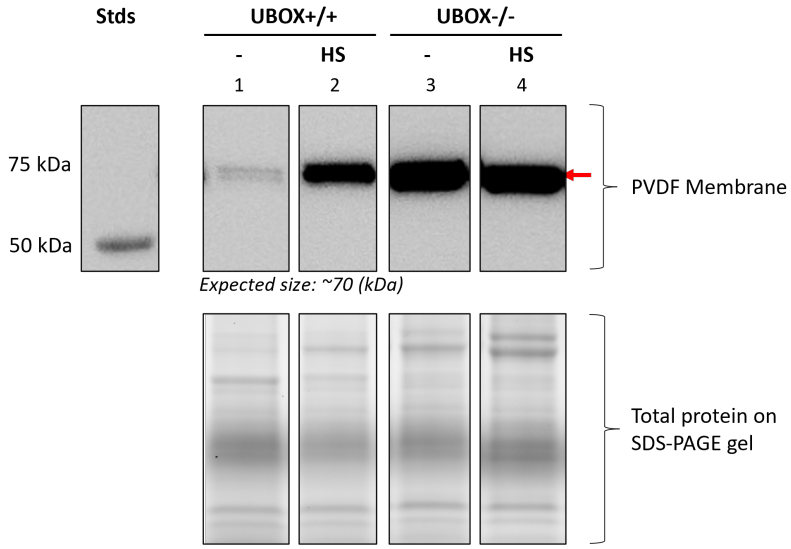

Figure 4.14: ***Hsc70/Hsp70 protein separation by western blot.*** *PVDF membrane (upper) stained with anti-Hsc70/Hsp70 (1:1000). The red arrow indicates Hsp70 proteins at approximately 70kDa. For the heat shocked mutant (-/-HS) a thick additional band can be seen at 120kDa. Smaller bands at 30 kDa were present in the wild-type samples (+/+ & +/+HS). The SDS-PAGE gel (lower) was run at 150V for 45 min, and is included to display the loaded protein amount. Stds: Unstained AllBlue, Ctrl: protein extracts from adult zebrafish brain tissue. UV exposure: 6 sec.*

The non-heat-shocked (Figure 4.14, indicated by -) wild-type (UBOX+/+) showed two weak bands at 70kDa , while the heat-shocked wild-type showed a strong band at the same size (HS). Both mutant (UBOX-/-) groups showed a strong band at 70kDa, where the non-heat-shocked mutant had a visibly stronger band than the non-heat-shocked wild-type. The quantification of the proteins better highlights these differences.

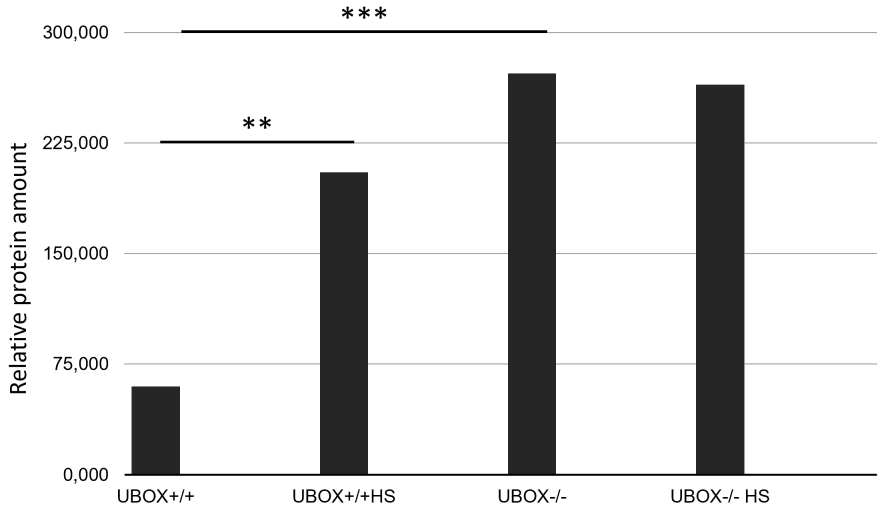

Figure 4.15: ***Hsc70/Hsp70 protein quantification from western blot.*** *Quantification by calculating the reference band:Hsp70 band ratio. A significantly higher amount of protein was seen in the wild-type with heat-shock compared to without (UBOX+/+HS and UBOX+/+, respectively). Similar protein amount in both mutant groups (UBOX-/- and UBOX-/-HS). A significantly higher protein amount was registered in the heat-shocked mutant than in the heat-shocked wild-type. Statistical method: Student's t-test, statistical significance indicated with asterisks (**p<0.01, ***p<0.001). n=3*

Quantification of the mean grey value is shown in Figure 4.15, and shows a significant increase in Hsp70 protein in the wild-type after heat shock compared to the non-heat-shocked wild-type sample. The Mutant showed no significant change between the heat-shocked and the non-heat-shocked samples, though there was a higher amount of Hsp70 protein in the heat-shocked mutant than in the heat-shocked wild-type.

5 Discussion

In this study, we investigated the Purkinje cell structure and HSR in homozygous U-box mutants. Our results show disorganisation of Purkinje cell dendrites in 3 year old zebrafish. A similar induction but slower termination of the HSR could be seen in the heat-shocked mutant samples, as *hsp70* and *hsp90* mRNA levels were lower in the wild-type after recovery. Hsp70 protein levels were higher in the mutant both with and without heat shock compared to the heat-shocked wild-type.

5.1 Investigation of the cerebellum and its Purkinje cells

The cerebellum was investigated because it has been shown that SCAR16 patients and mouse and zebrafish *STUB1* mutants display cerebellar atrophy and thinning of cerebellar folia (folds of the cerebellum that contain the characteristic cerebellum layers; ML, PCL and GCL) [62][63][7][64], with a decrease in Purkinje cell number [52][51]. For the U-box mutant, the phenotype analysis of 6 and 24 months old zebrafish showed that there was a negative trend for ML size in homozygous mutants, in addition to a decrease in Purkinje cell bodies [52]. To further investigate the progressiveness of NDs we studied the phenotype of the cerebellum in 3-year old zebrafish. Focusing on the Ce size, we observed a trend towards a decrease in the thickness of the ML in the mutant compared to the wild-type (Figure 4.3a). This trend was not statistically significant. However, the Ce : Ce + TeO ratio did not show any obvious trend of decrease in cerebellum size for the mutant (Figure 4.3b). Pakdaman *et al.* did not observe a decreasing trend in relative cerebellum size for the mutants [52]. We also counted the Purkinje cell bodies in the PCL (Figure 4.4). A trend could be seen, where the mutant displayed a lower number of cell bodies compared to the wild-type. The same trend has been observed before, in fish of both 6 and 24 months [52]. All together, our data point to a possible trend of cerebellar atrophy in the 36 months old U-box mutants.

Since SCAR16 and SCA48 are progressive NDs with symptoms such as atrophy that worsen over time, we would expect the morphological changes to be stronger in the 3-year old fish than in younger individuals studied before. We could not observe a statistically significant difference in the morphological aspects we investigated. In this study, three wild-type and three UBOX-/- fish were studied, but since there is a natural variation in

phenotypes between individuals, as there is in patients, a higher number of samples could give a clearer picture of the phenotypes. Another reason to repeat the experiments with more individuals is the detection of trends towards a decrease in ML size and Purkinje cell number. Increasing sample numbers of all ages could reveal statistical significant cerebellar phenotypes.

5.1.1 Purkinje cell dendrite morphology

SCAR16 is characterised by gait impairment and inability to fine-tune movement, we therefore next investigated the structure of the Purkinje cells in the cerebellum. They send signals through eurydendroid cells (DCN in mammals), which distribute it to other regions of the brain, making the Purkinje cells the only output neurons of the cerebellum. In addition, they can have as much as 100 000 connections to other neurons, more than any other neuron studied [65]. The dendrites of Purkinje cells have been shown to be highly branched and build an almost flat dendrite tree [63]. This dendrite tree originates in only one or two primary dendrites of the Purkinje cell, which makes them good models for studying orientation and branching patterning [66].

Pakdaman *et al.* have shown that at 24 months, the homozygous U-box mutant showed a less organised branching pattern [52]. On a sagittal section, wild-type dendrites tend to grow predominantly parallel to the PCL in the proximal half of the ML. In the distal half however, they grow more and more perpendicular to the PCL [52]. They found that there was a significant decrease in these perpendicularly oriented dendrites in the mutant. We analysed the branching pattern of dendrites to see if the same trends towards dendritic disorganisation that have been recorded for younger mutant individuals [52] can be seen in 36 month old fish. Our results largely overlap with what has been recorded by Pakdaman *et al.*. When quantifying the dendrite orientation in the ML of the posterior cerebellar region most distal to the PCL, we could see that the dendrites of the mutants were not predominantly perpendicular to the PCL (Figure 4.2). This means that far away from the PCL, a larger amount of dendrites branched parallel to the PCL in UBOX-/- fish than in UBOX+/+ fish. The difference was not statistically significant (Figure 4.5), but the reason for this could be the number of individuals studied.

5.1.2 CHIP in the cerebellum and Purkinje cells

CHIP has been shown to be highly present in Purkinje cells [12]. It has been shown that mice lacking CHIP display cerebellar degradation and have a lower tolerance for stress compared to wild-type mice [39]. We think that the direct link between Chip and the dendrite deformation might be bridged by the UPS, and that the loss of Chip could lead to protein aggregation to a level where the cells initiate apoptosis. Supporting this theory is for example the discovery that loss of the Parkin E3 ligase leads to accumulation of AIMP2 and FBBPl (Parkin substrates), which ultimately causes neurodegeneration [26].

E3 ligases such as Parkin and CHIP help maintain proteostasis by ubiquitinating non-native proteins for proteasomal degradation. In addition to being present in E3 ligases, U-box domains can also be found in E4 poly-ubiquitination enzymes, which polyubiquitinate already ubiquitinated substrates. Both E2 and E4 can act in absence of E3 [67]. In mice for example, the UFD2a E4 has been shown to be active in the cytoplasm of Purkinje cells, suggesting an alternative mechanism to CHIP-dependant ubiquitination in the UPS in our U-box mutant [68]. In wild-type conditions, an E4-like gain of function for CHIP, as suggested by Imai *et al.*, might increase CHIPs involvement in degradation [69]. They for example discovered that CHIP helps Parkin ubiquitinate Peal-R (an unfolded receptor) in order to prevent protein aggregation in one type if Parkinson's Disease. Little is known about the potential E4 function of CHIP, but we can hypothesise that the lack of both an E3 & E4 ligase function in Chip-mutants (as our U-box mutant) can have severe consequences for the amount of protein aggregates and ultimately cell survival.

Lack of CHIP may cause dendrite abnormalities through different manners. Several mechanisms must be in place for dendrite arbor development, homeostasis and remodelling. These are firstly: to form new, healthy dendrites, secondly: to maintain them, and thirdly: to degrade them. The endoplasmic reticulum (ER), present in Purkinje cell bodies, dendrites and axons, plays a vital role in dendrite formation [70]. A healthy ER ensures proper arborisation (branching) of dendrites [71]. If exposed to stress, excessive protein accumulations lead to malfunction of the ER. By activating the HSR through HSF1 activation and degradation of proteins in collaboration with the HSR-upregulated HSPs, CHIP indirectly ensures proper ER function [72]. For example, ER stress is induced by accumulation of α-synuclein in some forms of PD [73]. If, like in our homozygous U-box mutant, Chip cannot contribute to the degradation of protein aggregates (like α-synuclein)

and thereby preserve ER function, it might be one factor contributing to dendrite malformation. Not much is known about CHIPs function in the ER, but it would be interesting to investigate how much CHIP influences ER function, especially concerning NDs. It might be of interest to further investigate if there are other substrates whose degradation protects the ER, which might increase dendrite malformation in U-box mutants lacking Chips E3 ligase function.

The second aspect of dendrite branching is maintenance, for which the cytoskeleton has been shown to be central. Several HSPs have been shown to be involved, such as the small HSPs, a group of chaperones that help maintain normal arborisation in dendrites. For example in rats, HSPb5 and HSPb6 have been shown to increase dendritic complexity, while they also stabilise the cytoskeleton [74]. Another example is the control of proper tau-folding and turn-over, which is important in maintaining microtubule stability. In addition to being the cause of so-called tauopathies (NDs characterised by tau accumulation, one example is AD), tau levels have been found to be drastically increased in UBOX-/- mice [51]. HSC70/HSP70 have been found to lower abnormal tau levels by facilitating transport to the proteasome [75]. HSC70/HSP70 can however not facilitate ubiquitination without E3 ligases, and with Chip E3 function being abolished in our mutants, there might be accumulation of tau. We can hypothesise that its accumulation leads to formation of non-functional oligomeres, which might lead to cytoskeleton instability. There are more factors that affect dendrite stability in maintenance; trafficking of proteins, ribosomal subunits that are required for branching, and the Golgi apparatus, which makes it a complicated process to study [74].

Thirdly, protein degradation is important for regulating homeostasis and plasticity of synapses and the branching pattern, by ensuring protein turnover and for example dendrite pruning. Malfunctions in E3 ligases have been shown to affect dendrite arborisation. For example, the knockdown of the Ube3A E3 ligase in *Drosophila* causes a reduction in dendrite branching [76]. Since neurons are post-mitotic they can not eliminate waste by dividing, which makes them especially vulnerable to changes in proteostasis, such as a high number in protein aggregates [77]. Ubiquitination has been shown to occur in the dendrites of Purkinje cells [78]. Here, chaperones help in long term depression (LTD) of synapses, in which receptors to neurotransmitters (for example AMPA) are endocytosed to down-regulate the input from incoming synapses. This process has been shown to be

dependant on ubiquitination, where E3 ligases target these membrane receptors and facilitate degradation by the UPS. The specific mechanisms behind these are still unknown [79][74].

To conclude, there are many pathways through which CHIP might affect dendrite morphology that each offer hypotheses for how the loss of the E3 ligase function can affect the stability and branching pattern of the Purkinje cell dendrites. Our results show a less organised network of dendrites in the ML in the UBOX-/- mutant, and a previous study of 6 and 24 month old zebrafish has shown the same trends [52]. In addition, dendrite malformation is known to be a symptom in several other NDs, also involving malfunction of E3 ligases (PD, AD, Angelman syndrome) [76]. To specifically determine the pathways thorough with Chip is involved, one could focus on determining localisation of Chip and its substrates by IHC staining with specific antibodies. In addition to their localisation, one could investigate substrate amount e.g. of tau or α-synuclein. It could also be interesting to test this on heat-shocked individuals, to see how substrate amounts correlate with an increase in stress levels. In addition one could perform western blot on a native gel to investigate the amounts of substrate oligomeres in mutant and wild-type fish, with and without heat-shock.

E3 ligases normally localise in axons, dendrite cytoskeleton, synapses, nucleus, centrosome and Golgi apparatus of neurons [80]. CHIP on the other hand seems to have polarised expression, with localisation mostly in cell bodies and the proximal dendrites. In SCA48 patients, CHIP was found to also localise in the distal dendrites, but it is unknown how exactly this mislocalisation affects proteostasis and causes the phenotype of this dominant cerebellar ataxia [62].

5.2 The effect of heat stress on the HSR

Since a relatively mild zebrafish phenotype has been recorded compared to human SCAR16 patients and since NDs have been shown to be triggered by environmental stressors, we decided to have a closer look on the HSR. Here, CHIP plays the vital role of facilitating initiation of HSP transcription through helping HSF1 trimerise and where it plays the role of degrading the HSPs and HSF1 once the stress has passed [81]. Since HSF1 plays such a vital role in the HSR, any kind of inhibition/alteration of its function can be devastating for the cell environment.

5.2.1 Hsp90

Due to teleost-specific genome duplication (TSD) there are four *hsp90* paralogues in the zebrafish, and a significant increase in relative transcript could be seen in all of them at 60 min after heat-shock in both wild-type and mutant. The transcript levels increased the same amount in wild-types and mutants for *hsp90aa1.1* (Figure 4.10), *hsp90aa1.2* (Figure 4.11) and *hsp90ab1* (Figure 4.12). For *Hsp90b1* (Figure 4.13), the heat-shocked mutants had a lower relative expression than the heat-shocked wild-types. After 120 min *hsp90aa1.1* and *hsp90ab1* showed a significant increase in transcript levels in the treated mutant compared to the treated wild-type. This indicates a longer recovery time or failure to terminate the response in mutant samples compared to wild-types. The same trend could be seen in the other variants, though no statistical significance was calculated here. The increase in mRNA after heat shock does not fall in line with what has been discovered in adult zebrafish in previous studies. Murtha *et al.* found no increase in *hsp90* RNA levels following heat shock in adult wild-type zebrafish [82]. In rats on the other hand, Quraishi et al. found 1.5-fold and 2-3-fold induction of HSP90 in the cerebral hemisphere and cerebellum of heat-shocked individuals, respectively [83]. They also found a generally higher amount of *HSP90* mRNA in the cerebellum than cerebral hemisphere. It might be of interest to also investigate mRNA stability to better understand whether mRNA levels rise only due to an increase in transcription or if other factors (such as mRNA stability) affect mRNA longevity. The presence of a large amount of *hsp90* mRNA might mean that Hsp90 proteins accumulate faster. For our U-box mutant, which fails to degrade these efficiently, this might mean a negative influence on proteostasis which might lead to apoptosis or have an otherwise negative effect on the cell environment through altered feedback loops.

5.2.2 Hsp70

Murtha et al. have shown that *hsp70.1 and hsp70.3* RNA levels peak 30 min after heat shock in mature zebrafish, and those levels remained elevated for up to 4 hours [82]. Consistently, and similarly to our *hsp90* results, we discovered that the mRNA levels for all three *hsp70* paralogues were significantly higher in larvae exposed to heat-shock that those that remained at normal temperatures, for both mutants and wild-types (Figures 4.8 & 4.9). This might be explained by the fact that transcription induction increases

due to heat-shock, or possibly because mRNA stability of *hsp70* increases due to heat shock [84][85]. As for *hsp90*, it would be interesting to investigate the mRNA stability to assess how much of the increase is due to Hsf1 activation. In our study, *hsp70* transcript levels in the heat-shocked mutant at 60 min recovery were similar as in the heat-shocked wild-types. After 120 min recovery on the other hand, the heat-shocked mutants showed a significantly higher level of *hsp70* transcripts than the heat-shocked wild-types. This indicates a longer recovery period in the mutant compared to the wild-type, as was also seen for *hsp90* transcript levels.

In addition, it has been shown that protein stability increases during heat shock. In mouse CHIP(H260Q) fibroblasts (lacking E3 ligase activity), there were higher basal levels of HSP70, which was sustained even after heat shock [86]. Both the higher basal levels and the increased protein stability during heat shock might contribute to a constant stress situation in which accumulations of proteins potentially inhibit cellular functions. Our results show that for the mutants, there is a relatively low level of *hsp70* transcripts without the heat shock. Yet, there are high levels of Hsp70 protein (Figure 4.14). The heat-shocked mutants showed a higher transcript level, but the same amount of protein as the untreated mutants. As we can see, there is initiation of *hsp70* transcription by Hsf1 due to heat-shock. Hsp70 protein levels in the mutants do not seem to be regulated during the recovery period, probably due to the non-functionality of Chips U-box. One can hypothesise that *hsp70* transcript levels decrease during the recovery period even in the mutant, though with a delay, which might be due to the accumulation of Hsp proteins in the mutant.

5.2.3 Hsf1

Monomeric HSF1 is at all times present in the cell, and upon stress (such as heat), CHIP facilitates its nuclear translocation and trimerisation. Once trimerised, HSF1 initiates *HSP* transcription. The trimerisation of HSF1 is facilitated by CHIP, but in Drosophila and humans, purified HSF1 has been shown to trimerise spontaneously in response to an increase in temperature or oxidative stress. This might be a result of structural changes due to heat, which might expose trimerisation domains [87]. The recruitment of HSP70 and HSP90 away from HSF1 by the presence of non-native proteins also removes the inhibition on HSF1.

Our western blot results show an increase in Hsp70 proteins after heat shock in the wild-type, while the mutant samples showed no significant change in protein levels. The UBOX-/- mutant Chip contains a truncated U-box, but the TPR at Chips N-terminus is still intact. Hence, the transport and trimerisation of Hsf1, and with it, *hsp70* transcription could be maintained. During attenuation of the HSR, Hsp70 (but not Hsp90) helps disassociate HSF1 from the HSE, creating a negative feedback loop on its own protein levels. The degradation of Hsf1 protein is mediated by Hsp70 and E3-ligases such as Chip [88]. The lack of Chip could therefore lead to impaired Hsf1 degradation, leading to a delayed recovery and possible abnormalities in the negative feedback loop. It is important to note that E3 ligases such as FBWX7, have been shown to help degrade HSF1 in cancer models, in which there is an overflow of HSF1 [33][89], hinting at other pathways through which HSF1 and the HSPs can be degraded independently of CHIP. To investigate the connection between *hsf1* mRNA and protein levels it would be interesting to also perform western blot to detect Hsf1 protein levels in the U-box mutant.

5.2.4 The importance of the CHIP U-box domain

CHIP plays an important role in the HSR; it facilitates both initiation and recovery. Its regulation is therefore important for maintenance of cellular homeostasis.

The U-box at the C-terminus seems to be highly important in CHIP-folding, stabilisation, dimerisation and self-ubiquitination [14]. Ye *et al.* found that by removing the last 6 amino acids in the C-terminus, and thereby truncating the U-box, ubiquitination of substrates was significantly lowered and Chips auto-ubiquitinating function was absent. Pakdaman *et al.* have shown that Chips self-ubiquitination function was absent in T246M mutants, which have an abolished U-box function [9]. The same trend has been shown to be present in zebrafish G249V mutants (also abolishing U-box function), where there was an impaired ubiquitination of both Hsc70 and Chip itself [14][90]. Similar to these other studies, our results showed an increase in *hsp70/90* mRNA in the heat-shocked mutants compared to the heat-hocked wild-types, which points towards maintained Hsf1 trans-localisation and possibly increased co-chaperone interaction with Hsp70, even with a truncated U-box (Figures 4.8 & 4.9). Levels of *hsp70/90* mRNA also showed a trend towards delayed recovery in the heat-shocked mutants compared to the wild-types (Figures 4.10,4.11,4.12 and 4.13). This indicates a prolonged stress situation in the cells, which

in wild-types samples seems to be shorter as a result of the presence of Chips U-Box. Transcript levels of *hsf1* were only different between heat-shocked mutant and wild-type samples at 60 min, pointing towards transcriptional control of *hsf1* independent of Chip and the abolished U-box function in our mutant (Figure 4.7). Hsp70 protein levels were elevated in the mutants compared to the wild-types, both in the heat-shocked and in the non-heat-shocked samples Figure (Figure 4.15). As for the transcript levels of *hsp70/90*, these elevated Hsp70 protein levels point towards a prolonged stress situation in the cells, which can't seem to degrade Hsp70 in the absence of a functional U-box in Chip.

One mechanism that affects Chip function is its dimerisation. Dimer formation is necessary for proper functionality, and it has been shown that not only the HH region is needed for proper dimerisation, but also the U-box after HH-interactions have been established [13]. This U-box interaction causes the asymmetric structure of CHIP in both mammals and zebrafish, in which only one of the U-boxes is functional, while the other is blocked by a TPR domain [14]. We can consider that heterodimerisation in heterozygous *stub1* mutants might result in a dominant-negative version of CHIP, where the TPR is functional but not the U-box. Investigating the possibility of a similar mechanism in SCA48 patients would be interesting, but there is currently too little knowledge about the behaviour of heterodimerised CHIP and the mechanisms behind SCA48.

It is important to note that CHIP also has been found to play a role in the autophagy pathway, where CHIP knock-down has been shown to inhibit autophagic flux (autophagic degradation activity), thereby increasing the accumulation of autophagosomes (spherical double membrane structure that delivers substrates to the lysosome) [91]. U-box mutations might thereby not only influence Chips functionality, but also the balance between the two pathways.

5.3 The effect of environmental factors on the brain and Purkinje cells

NDs have been shown to increase the cells sensitivity to environmental stressors. Humans are exposed to environmental stressors of different sorts, and it has been shown that toxicants can speed up the progression of underlying NDs. Oxidative stress caused by accumulation of free radicals such as reactive oxygen species (ROS) leads to the formation of amyloid-β sheets in AD and α-synuclein accumulation in PD. The brain uses 1/5 of

the oxygen circulating the body, which makes it more prone to oxidative stress. There is also a lower level of antioxidants in the brain, in addition to a higher level of metals (e.g. iron) which can increase ROS formation [1]. Purkinje cells are especially vulnerable to stressors, as mentioned earlier, and it is not unthinkable that the Purkinje cells also have an adapted amount of transcripts to handle stress situations. Especially heat has been shown to damage Purkinje cells. This leads to an upregulation in HSPs, which can also be seen as a response to ER stress and oxidative stress [74]. All of these stressors have been shown to damage Purkinje cell development, growth, arborisation and maintenance.

Different stressors may affect SCAR16 patients in different manners, since CHIP interacts with a wide variety of other proteins. We tested the effect of heat-shock on zebrafish larvae to analyse the HSR. It would also be interesting to do the experiment on adult zebrafish, and analyse the correlation with the different branching pattern that we observed in the UBOX-/- mutants. It has been proposed that the HSR is not induced in neurons *in vitro* [77]. However, Carnemolla et al. failed to replicate these results *in vivo* in mice [92]. Schuster *et al.* exposed cortical neurons derived from induced pluripotent stem cells (iPSC) of SCAR16 patients to heat shock and measured the transcript and protein levels. Surprisingly, they found out that neurons in the CNS had a high basal level of HSPs compared to fibroblasts, but they did not find an increase in HSP protein levels. All of these studies suggest that there is uncertainty around whether the HSR is induced in neurons, and if so, how strongly. In addition, an increase in *HSP70* mRNA in iPSC neurons and adult zebrafish brain tissue has been reported due to heat shock [28][82]. In humans, fever and inhibited cooling mechanisms due to dehydration cause heat stress. In these situations, Hsf1 maintains proteostasis to prevent aggregation [33]. In SCAR16 patients, the HSR might be strongly impaired due to the truncation of CHIPs U-box domain, leading to accumulation of non-native proteins and subsequently apoptosis. It is important to notice that we did not analyse the HSR in a tissue-specific manner in the 5dpf larvae, but it would be of interest to investigate this in future studies.

In the brain, CHIP substrates are involved in many pathways that maintain normal cell functionality: tau is involved with the ER; amyloid-β are short peptides which are degraded with the help of CHIP to reduce their toxicity; the accumulation of α-synuclein has negative affects on the UPS. Different types of autophagy are effected by CHIP malfunction, along with functions of the ER, Golgi apparatus, and mitochondria [93].

In addition, the HSR is dependant on CHIP-mediated translocation and trimerisation of HSF1.

5.4 Conclusion

In this study, we characterised the effect of stub1 UBOX-/- mutation on adult cerebellum structure and on HSR in 5dpf larvae. Using parvalbumin as a marker for Purkinje cells and dendrite branching direction quantification, it was shown that 3 year old zebrafish UBOX-/- mutants had a less organised dendrite branching pattern. RT-qPCR analysis on 5dpf zebrafish larvae exposed to 60 min 38°C heat shock, showed that HSR initiation is present in both wild-types and mutants, as *hsf1* levels were elevated to a similar extend in both wild-types and mutants after heat-shock. This indicated transcriptional regulation of *hsf1* by other mechanisms than those involving Chips U-box. HSR termination and recovery were delayed in the mutant as could be seen from higher *hsp70* and *hsp90* transcript levels after 120 min in the heat-shocked mutant compared to the heat-shocked wild-type. Elevated Hsp70 protein levels after 60 min recovery in the mutant compared to the wild-type and an elevated level of Hsp protein under non-heat-shock conditions in the mutant indicate impaired degradation usually facilitated by Chips U-box domain.

5.5 Future Prospects

Our heat shock experiments have been performed at two time points to measure transcript and protein levels during the recovery period, additional time-points would improve the analysis. In particular, sampling directly after heat shock, and after 30 min would have given us a better idea of how fast the HSR is initiated. Looking at heterozygous U-box mutants would also be interesting to confirm our hypothesis of a dominant-negative effect of the U-box mutation. It would also be wise to investigate the heat shock in adult individuals, and subsequently analyse dendrite structure to directly create a link between morphological changes in the cerebellum and the HSR. Testing other stressors will also help understand the extent to which truncation of the U-box can lead to neurodegeneration (for example exposure to chemicals, which might have a larger effect).In addition, it would be interesting to investigate how a Chip null mutant would react to stressors, and how cerebellar structure is affected. It has been shown that CHIP-/- mice die during or within 4 hours of heat shock for example [39]. Behavioural analysis of UBOX-/- zebrafish

have shown that they express less anxiety, contrary to the phenotype seen in humans. It would therefore be interesting to also compare Chip-/- zebrafish behaviour to both human phenotypes and to other Chip mutants.

Limitations to our study were for example zebrafish egg availability for heat shock experiments, in particular for protein analysis. The fish that were used for egg production were relatively old, just under two years, which might have influenced the number of eggs they produced, and starting new generation would be necessary for future studies. For the dendrite structure analysis on adult zebrafish, we realised after genotyping that the number of 3 year old homozygous individuals was low, limiting the power of statistical analysis.

References

[1] L Migliore and F Coppede. Environmental-induced oxidative stress in neurodegenerative disorders and aging. *MUTATION RESEARCH-GENETIC TOXICOLOGY AND ENVIRONMENTAL MUTAGENESIS*, 674(1-2):73–84, 2009.

[2] A J Kanack, O J Newsom, and K M Scaglione. Most mutations that cause spinocerebellar ataxia autosomal recessive type 16 (SCAR16) destabilize the protein quality-control E3 ligase CHIP. *JOURNAL OF BIOLOGICAL CHEMISTRY*, 293(8):2735–2743, 2018.

[3] A Ciechanover and Y T Kwon. Protein Quality Control by Molecular Chaperones in Neurodegeneration. *FRONTIERS IN NEUROSCIENCE*, 11, 2017.

[4] J D Schmahmann. Disorders of the cerebellum: Ataxia, dysmetria of thought, and the cerebellar cognitive affective syndrome. *JOURNAL OF NEUROPSYCHIATRY AND CLINICAL NEUROSCIENCES*, 16(3):367–378, 2004.

[5] P Cabaraux, J Gandini, S Kakei, M Manto, H Mitoma, and H Tanaka. Dysmetria and Errors in Predictions: The Role of Internal Forward Model. *INTERNATIONAL JOURNAL OF MOLECULAR SCIENCES*, 21(18), 2020.

[6] M Manto and D Marmolino. Cerebellar ataxias. *CURRENT OPINION IN NEUROLOGY*, 22(4):419–429, 2009.

[7] H H Chiu, C T Hsaio, Y S Tsai, Y C Liao, Y C Lee, and B W Soong. Clinical and Genetic Characterization of Autosomal Recessive Spinocerebellar Ataxia Type 16 (SCAR16) in Taiwan. *CEREBELLUM*, 19(4):544–549, 2020.

[8] D Genis, S Ortega-Cubero, H San Nicolas, J Corral, J Gardenyes, L de Jorge, E Lopez, B Campos, E Lorenzo, R Tonda, S Beltran, M Negre, M Obon, B Beltran, L Fabregas, B Alemany, F Marquez, L Ramio-Torrenta, J Gich, V Volpini, and P Pastor. Heterozygous STUB1 mutation causes familial ataxia with cognitive affective syndrome (SCA48). *Neurology*, 91(21):E1988–E1998, 2018.

[9] Y Pakdaman, M Sanchez-Guixe, R Kleppe, S Erdal, H J Bustad, L Bjrkhaug, K Haugarvoll, C Tzoulis, K Heimdal, P M Knappskog, S Johansson, and I Aukrust. In vitro

characterization of six STUB1 variants in spinocerebellar ataxia 16 reveals altered structural properties for the encoded CHIP proteins. *Bioscience Reports*, 37:12, 2017.

[10] G De Michele, D Galatolo, M Barghigiani, D Dello Iacovo, R Trovato, A Tessa, E Salvatore, A Filla, G De Michele, and F M Santorelli. Spinocerebellar ataxia type 48: last but not least. *Neurological Sciences*, 41(9):2423–2432, 2020.

[11] I Paul and M K Ghosh. The E3 Ligase CHIP: Insights into Its Structure and Regulation. *BIOMED RESEARCH INTERNATIONAL*, 2014, 2014.

[12] C A Ballinger, P Connell, Y X Wu, Z Y Hu, L J Thompson, L Y Yin, and C Patterson. Identification of CHIP, a novel tetratricopeptide repeat-containing protein that interacts with heat shock proteins and negatively regulates chaperone functions. *Molecular and Cellular Biology*, 19(6):4535–4545, 1999.

[13] R Nikolay, T Wiederkehr, W Rist, G Kramer, M P Mayer, and B Bukau. Dimerization of the human E3 ligase CHIP via a coiled-coil domain is essential for its activity. *Journal of Biological Chemistry*, 279(4):2673–2678, 2004.

[14] Z F Ye, P G Needham, S K Estabrooks, S K Whitaker, B L Garcia, S Misra, J L Brodsky, and C J Camacho. Symmetry breaking during homodimeric assembly activates an E3 ubiquitin ligase. *Scientific Reports*, 7:9, 2017.

[15] M H Zhang, M Windheim, S M Roe, M Peggie, P Cohen, C Prodromou, and L H Pearl. Chaperoned ubiquitylation - Crystal structures of the CHIPU box E3 ubiquitin ligase and a CHIP-Ubc13-Uev1a complex. *Molecular Cell*, 20(4):525–538, 2005.

[16] A R Dubey, S M Patwa, S Kinger, Y A Jagtap, P Kumar, S Singh, R Dhiman, H C Jha, and A Mishra. Improper Proteostasis: Can It Serve as Biomarkers for Neurodegenerative Diseases? *MOLECULAR NEUROBIOLOGY*, 2022.

[17] J W Kelly. Alternative conformations of amyloidogenic proteins govern their behavior. *CURRENT OPINION IN STRUCTURAL BIOLOGY*, 6(1):11–17, 1996.

[18] D H Lee and A L Goldberg. Proteasome inhibitors: valuable new tools for cell biologists. *TRENDS IN CELL BIOLOGY*, 8(10):397–403, 1998.

[19] J Labbadia and R I Morimoto. The Biology of Proteostasis in Aging and Disease. In R D Kornberg, editor, *ANNUAL REVIEW OF BIOCHEMISTRY, VOL 84*, volume 84, pages 435–464. Northwestern Univ, Rice Inst Biomed Res, Dept Mol Biosci, Evanston, IL 60208 USA FU - NATIONAL INSTITUTE OF GENERAL MEDICAL SCIENCESUnited States Department of Health & Human ServicesNational Institutes of Health (NIH) - USANIH National Institute of Gener, 2015.

[20] Q A Huang and M E Figueiredo-Pereira. Ubiquitin/proteasome pathway impairment in neurodegeneration: therapeutic implications. *APOPTOSIS*, 15(11):1292–1311, 2010.

[21] L Aravind and E V Koonin. The U box is a modified RING finger - a common domain in ubiquitination. *CURRENT BIOLOGY*, 10(4):R132–R134, 2000.

[22] M Koegl, T Hoppe, S Schlenker, H D Ulrich, T U Mayer, and S Jentsch. A novel ubiquitination factor, E4, is involved in multiubiquitin chain assembly. *CELL*, 96(5):635–644, 1999.

[23] A Hershko and A Ciechanover. The ubiquitin system. *ANNUAL REVIEW OF BIOCHEMISTRY*, 67:425–479, 1998.

[24] Rachel E Lackie, Andrzej Maciejewski, Valeriy G Ostapchenko, Jose Marques-Lopes, Wing-Yiu Choy, Martin L Duennwald, Vania F Prado, and Marco A M Prado. The Hsp70/Hsp90 Chaperone Machinery in Neurodegenerative Diseases. *Frontiers in Neuroscience*, 11:254, 2017.

[25] R J Miller and S M Wilson. Neurological disease: UPS stops delivering! *TRENDS IN PHARMACOLOGICAL SCIENCES*, 24(1):18–23, 2003.

[26] T M Dawson and V L Dawson. The Role of Parkin in Familial and Sporadic Parkinson's Disease. *MOVEMENT DISORDERS*, 25(3):S32–S39, 2010.

[27] N Zheng and N Shabek. Ubiquitin Ligases: Structure, Function, and Regulation. In R D Kornberg, editor, *ANNUAL REVIEW OF BIOCHEMISTRY, VOL 86*, volume 86, pages 129–157. Univ Washington, Howard Hughes Med Inst, Seattle, WA 98195 USA, 2017.

[28] S Schuster, E Heuten, A Velic, J Admard, M Synofzik, S Ossowski, B Macek, S Hauser, and L Schols. CHIP mutations affect the heat shock response differently in human fibroblasts and iPSC-derived neurons. *DISEASE MODELS & MECHANISMS*, 13(10), 2020.

[29] C Graf, M Stankiewicz, R Nikolay, and M P Mayer. Insights into the Conformational Dynamics of the E3 Ubiquitin Ligase CHIP in Complex with Chaperones and E2 Enzymes. *Biochemistry*, 49(10):2121–2129, 2010.

[30] David Pincus. Regulation of Hsf1 and the Heat Shock Response. In Marc Laurence Mendillo, David Pincus, and Ruth Scherz-Shouval, editors, *HSF1 and Molecular Chaperones in Biology and Cancer*, pages 41–50. Springer International Publishing, Cham, 2020.

[31] B J Lang, M E Guerrero, T L Prince, Y Okusha, C Bonorino, and S K Calderwood. The functions and regulation of heat shock proteins; key orchestrators of proteostasis and the heat shock response. *ARCHIVES OF TOXICOLOGY*, 95(6):1943–1970, 2021.

[32] K Richter, M Haslbeck, and J Buchner. The Heat Shock Response: Life on the Verge of Death. *MOLECULAR CELL*, 40(2):253–266, 2010.

[33] S W Kmiecik and M P Mayer. Molecular mechanisms of heat shock factor 1 regulation. *TRENDS IN BIOCHEMICAL SCIENCES*, 47(3):218–234, 2022.

[34] X Zheng, J Krakowiak, N Patel, A Beyzavi, J Ezike, A S Khalil, and D Pincus. Dynamic control of Hsf1 during heat shock by a chaperone switch and phosphorylation. *ELIFE*, 5, 2016.

[35] A E Masser, M Ciccarelli, and C Andreasson. Hsf1 on a leash - controlling the heat shock response by chaperone titration. *EXPERIMENTAL CELL RESEARCH*, 396(1), 2020.

[36] D W Neef, A M Jaeger, and D J Thiele. Heat shock transcription factor 1 as a therapeutic target in neurodegenerative diseases. *NATURE REVIEWS DRUG DISCOVERY*, 10(12):930–944, 2011.

[37] S Zwirowski, A Klosowska, I Obuchowski, N B Nillegoda, A Pirog, S Zietkiewicz, B Bukau, A Mogk, and K Liberek. Hsp70 displaces small heat shock proteins from aggregates to initiate protein refolding. *EMBO JOURNAL*, 36(6):783–796, 2017.

[38] X C Zeng, S Bhasin, X F Wu, J G Lee, S Maffi, C J Nichols, K J Lee, J P Taylor, L E Greene, and E Eisenberg. Hsp70 dynamics in vivo: effect of heat shock and protein aggregation. *JOURNAL OF CELL SCIENCE*, 117(21):4991–5000, 2004.

[39] Q Dai, C L Zhang, Y X Wu, H McDonough, R A Whaley, V Godfrey, H H Li, N Madamanchi, W Xu, L Neckers, D Cyr, and C Patterson. CHIP activates HSF1 and confers protection against apoptosis and cellular stress. *Embo Journal*, 22(20):5446–5458, 2003.

[40] R I Morimoto. Regulation of the heat shock transcriptional response: cross talk between a family of heat shock factors, molecular chaperones, and negative regulators. *GENES & DEVELOPMENT*, 12(24):3788–3796, 1998.

[41] K Adelman and J T Lis. Promoter-proximal pausing of RNA polymerase II: emerging roles in metazoans. *NATURE REVIEWS GENETICS*, 13(10):720–731, 2012.

[42] S Raychaudhuri, C Loew, R Korner, S Pinkert, M Theis, M Hayer-Hartl, F Buchholz, and F U Hartl. Interplay of Acetyltransferase EP300 and the Proteasome System in Regulating Heat Shock Transcription Factor 1. *CELL*, 156(5):975–985, 2014.

[43] G S Gerhard. Comparative aspects of zebrafish (Danio rerio) as a model for aging research. *EXPERIMENTAL GERONTOLOGY*, 38(11-12):1333–1341, 2003.

[44] A S Glass and R Dahm. The zebrafish as a model organism for eye development. *OPHTHALMIC RESEARCH*, 36(1):4–24, 2004.

[45] W C Shi, Z B Fang, L Li, and L F Luo. Using zebrafish as the model organism to understand organ regeneration. *SCIENCE CHINA-LIFE SCIENCES*, 58(4):343–351, 2015.

[46] J Ablain and L I Zon. Of fish and men: using zebrafish to fight human diseases. *TRENDS IN CELL BIOLOGY*, 23(12):584–586, 2013.

[47] B Schmid and C Haass. Genomic editing open new avenues for zebrafish as a model for neurodegeneration. *JOURNAL OF NEUROCHEMISTRY*, 127(4):461–470, 2013.

[48] K Howe, M D Clark, C F Torroja, J Torrance, C Berthelot, M Muffato, J E Collins, and Et Al. The zebrafish reference genome sequence and its relationship to the human genome. *Nature*, 496(7446):498–503, 2013.

[49] A V Kalueff, A M Stewart, and R Gerlai. Zebrafish as an emerging model for studying complex brain disorders. *TRENDS IN PHARMACOLOGICAL SCIENCES*, 35(2):63–75, 2014.

[50] S C Madrigal, Z McNeil, R Sanchez-Hodge, C H Shi, C Patterson, K M Scaglione, and J C Schisler. Changes in protein function underlie the disease spectrum in patients with CHIP mutations. *JOURNAL OF BIOLOGICAL CHEMISTRY*, 294(50):19236–19245, 2019.

[51] C H Shi, C Rubel, S E Soss, R Sanchez-Hodge, S Zhang, S C Madrigal, S Ravi, H McDonough, R C Page, W J Chazin, C Patterson, C Y Mao, M S Willis, H Y Luo, Y S Li, D A Stevens, M B Tang, P Du, Y H Wang, Z W Hu, Y M Xu, and J C Schisler. Disrupted structure and aberrant function of CHIP mediates the loss of motor and cognitive function in preclinical models of SCAR16. *Plos Genetics*, 14(9):36, 2018.

[52] Y Pakdaman, E Denker, E Austad, W H J Norton, H O Rolfsnes, L A Bindoff, C Tzoulis, I Aukrust, P M Knappskog, S Johansson, and S Ellingsen. Chip Protein U-Box Domain Truncation Affects Purkinje Neuron Morphology and Leads to Behavioral Changes in Zebrafish. *FRONTIERS IN MOLECULAR NEUROSCIENCE*, 14, 2021.

[53] Y K Bae, S Kani, T Shimizu, K Tanabe, H Nojima, Y Kimura, S Higashijima, and M Hibi. Anatomy of zebrafish cerebellum and screen for mutations affecting its development. *DEVELOPMENTAL BIOLOGY*, 330(2):406–426, 2009.

[54] M Hibi and T Shimizu. Development of the cerebellum and cerebellar neural circuits. *DEVELOPMENTAL NEUROBIOLOGY*, 72(3):282–301, 2012.

[55] K Fujishima, K K Galbraith, and M Kengaku. Dendritic Self-Avoidance and Morphological Development of Cerebellar Purkinje Cells. *CEREBELLUM*, 17(6):701–708, 2018.

[56] Alyna Katti, Bianca J Diaz, Christina M Caragine, Neville E Sanjana, and Lukas E Dow. CRISPR in cancer biology and therapy. *Nature Reviews Cancer*, 2022.

[57] P D Hsu, E S Lander, and F Zhang. Development and Applications of CRISPR-Cas9 for Genome Engineering. *CELL*, 157(6):1262–1278, 2014.

[58] P Alestrom, L D'Angelo, P J Midtlyng, D F Schorderet, S Schulte-Merker, F Sohm, and S Warner. Zebrafish: Housing and husbandry recommendations. *LABORATORY ANIMALS*, 54(3):213–224, 2020.

[59] M W Pfaffl. A new mathematical model for relative quantification in real-time RT-PCR. *NUCLEIC ACIDS RESEARCH*, 29(9), 2001.

[60] K R Vinod, D Jones, and V Udupa. A simple and effective heat induced antigen retrieval method. *Methodsx*, 3:315–319, 2016.

[61] Novus Biologicals. Antigen Retrieval Protocol (HIER).

[62] D H Chen, C Latimer, M Yagi, M K Ndugga-Kabuye, E Heigham, S Jayadev, J S Meabon, C M Gomez, C D Keene, D G Cook, W H Raskind, and T D Bird. Heterozygous STUB1 missense variants cause ataxia, cognitive decline, and STUB1 mislocalization. *Neurology-Genetics*, 6(2):13, 2020.

[63] J P Kapfhammer. Cellular and molecular control of dendritic growth and development of cerebellar Purkinje cells. *PROGRESS IN HISTOCHEMISTRY AND CYTOCHEMISTRY*, 39(3):131–182, 2004.

[64] J M Ravel, M Benkirane, N Calmels, C Marelli, F Ory-Magne, C Ewenczyk, Y Halleb, F Tison, C Lecocq, G Pische, P Casenave, A Chaussenot, S Frismand, L Tyvaert, L Larrieu, M Pointaux, N Drouot, C Bossenmeyer-Pourie, A Oussalah, J L Gueant, B Leheup, C Bonnet, M Anheim, C Tranchant, L Lambert, J Chelly, M Koenig, and M Renaud. Expanding the clinical spectrum of STIP1 homology and U-box containing protein 1-associated ataxia. *Journal of Neurology*, 268(5):1927–1937, 2021.

[65] Scott F. Gilbert and Michael J. F. Barresi. *Developmental Biology*. Oxford University Press, 11 edition, 2018.

[66] K Tanabe, S Kani, T Shimizu, Y K Bae, T Abe, and M Hibi. Atypical Protein Kinase C Regulates Primary Dendrite Specification of Cerebellar Purkinje Cells by Localizing Golgi Apparatus. *JOURNAL OF NEUROSCIENCE*, 30(50):16983–16992, 2010.

[67] S Hatakeyama, M Yada, M Matsumoto, N Ishida, and K I Nakayama. U box proteins as a new family of ubiquitin-protein ligases. *JOURNAL OF BIOLOGICAL CHEMISTRY*, 276(35):33111–33120, 2001.

[68] C Kaneko, S Hatakeyama, M Matsumoto, M Yada, K Nakayama, and K I Nakayama. Characterization of the mouse gene for the U-box-type ubiquitin lipase UFD2a. *BIOCHEMICAL AND BIOPHYSICAL RESEARCH COMMUNICATIONS*, 300(2):297–304, 2003.

[69] Y Imai, M Soda, S Hatakeyama, T Akagi, T Hashikawa, K Nakayama, and R Takahashi. CHIP is associated with Parkin, a gene responsible for familial Parkinson's disease, and enhances its ubiquitin ligase activity. *MOLECULAR CELL*, 10(1):55–67, 2002.

[70] M TERASAKI, N T SLATER, A FEIN, A SCHMIDEK, and T S REESE. CONTINUOUS NETWORK OF ENDOPLASMIC-RETICULUM IN CEREBELLAR PURKINJE NEURONS. *PROCEEDINGS OF THE NATIONAL ACADEMY OF SCIENCES OF THE UNITED STATES OF AMERICA*, 91(16):7510–7514, 1994.

[71] T T Cui-Wang, C Hanus, T Cui, T Helton, J Bourne, D Watson, K M Harris, and M D Ehlers. Local Zones of Endoplasmic Reticulum Complexity Confine Cargo in Neuronal Dendrites. *CELL*, 148(1-2):309–321, 2012.

[72] Y Liu and A Chang. Heat shock response relieves ER stress. *EMBO JOURNAL*, 27(7):1049–1059, 2008.

[73] T Wang and J C Hay. Alpha-synuclein Toxicity in the Early Secretory Pathway: How It Drives Neurodegeneration in Parkinsons Disease. *FRONTIERS IN NEUROSCIENCE*, 9, 2015.

[74] E N Lottes and D N Cox. Homeostatic Roles of the Proteostasis Network in Dendrites. *FRONTIERS IN CELLULAR NEUROSCIENCE*, 14, 2020.

[75] J Abisambra, U K Jinwal, Y Miyata, J Rogers, L Blair, X Li, S P Seguin, L Wang, Y Jin, J Bacon, S Brady, M Cockman, C Guidi, J Zhang, J Koren, Z T Young, C A Atkins, B Zhang, L Y Lawson, E J Weeber, J L Brodsky, J E Gestwicki, and C A Dickey. Allosteric Heat Shock Protein 70 Inhibitors Rapidly Rescue Synaptic Plasticity Deficits by Reducing Aberrant Tau. *BIOLOGICAL PSYCHIATRY*, 74(5):367–374, 2013.

[76] Y B Lu, F Wang, Y Li, J Ferris, J A Lee, and F B Gao. The Drosophila homologue of the Angelman syndrome ubiquitin ligase regulates the formation of terminal dendritic branches. *HUMAN MOLECULAR GENETICS*, 18(3):454–462, 2009.

[77] J H Son, J H Shim, K H Kim, J Y Ha, and J Y Han. Neuronal autophagy and neurodegenerative diseases. *EXPERIMENTAL AND MOLECULAR MEDICINE*, 44(2):89–98, 2012.

[78] S Flann, R B Hawkes, B M Riederer, C C Rider, and P W Beesley. Changes in ubiquitin immunoreactivity in developing rat brain: A putative role for ubiquitin and ubiquitin conjugates in dendrite outgrowth and differentiation. *NEUROSCIENCE*, 81(1):173–187, 1997.

[79] C Piochon, M Kano, and C Hansel. LTD-like molecular pathways in developmental synaptic pruning. *NATURE NEUROSCIENCE*, 19(10):1299–1310, 2016.

[80] T Yamada, Y Yang, and A Bonni. Spatial organization of ubiquitin ligase pathways orchestrates neuronal connectivity. *TRENDS IN NEUROSCIENCES*, 36(4):218–226, 2013.

[81] C Y Huang, W W Kuo, J F Lo, T J Ho, P Y Pai, S F Chiang, P Y Chen, F J Tsai, C H Tsai, and C Y Huang. Doxorubicin attenuates CHIP-guarded HSF1 nuclear translocation and protein stability to trigger IGF-IIR-dependent cardiomyocyte death. *CELL DEATH & DISEASE*, 7, 2016.

[82] J M Murtha and E T Keller. Characterization of the heat shock response in mature zebrafish (Danio rerio). *EXPERIMENTAL GERONTOLOGY*, 38(6):683–691, 2003.

[83] H Quraishi, S J Rush, and I R Brown. Expression of mRNA species encoding heat shock protein 90 (hsp90) in control and hyperthermic rabbit brain. *JOURNAL OF NEUROSCIENCE RESEARCH*, 43(3):335–345, 1996.

[84] K Kaarniranta, M Elo, R Sironen, M J Lammi, M B Goldring, J E Eriksson, L Sistonen, and H J Helminen. Hsp70 accumulation in chondrocytic cells exposed to high continuous hydrostatic pressure coincides with mRNA stabilization rather than transcriptional activation. *PROCEEDINGS OF THE NATIONAL ACADEMY OF SCIENCES OF THE UNITED STATES OF AMERICA*, 95(5):2319–2324, 1998.

[85] N G THEODORAKIS and R I MORIMOTO. POSTTRANSCRIPTIONAL REGULATION OF HSP70 EXPRESSION IN HUMAN-CELLS - EFFECTS OF HEAT-SHOCK, INHIBITION OF PROTEIN-SYNTHESIS, AND ADENOVIRUS INFECTION ON TRANSLATION AND MESSENGER-RNA STABILITY. *MOLECULAR AND CELLULAR BIOLOGY*, 7(12):4357–4368, 1987.

[86] S B Qian, H McDonough, F Boellmann, D M Cyr, and C Patterson. CHIP-mediated stress recovery by sequential ubiquitination of substrates and Hsp70. *Nature*, 440(7083):551–555, 2006.

[87] M Zhong, A Orosz, and C Wu. Direct sensing of heat and oxidation by Drosophila heat shock transcription factor. *MOLECULAR CELL*, 2(1):101–108, 1998.

[88] S W Kmiecik, L Le Breton, and M P Mayer. Feedback regulation of heat shock factor 1 (Hsf1) activity by Hsp70-mediated trimer unzipping and dissociation from DNA. *EMBO JOURNAL*, 39(14), 2020.

[89] S Daakour, L J Hajingabo, D Kerselidou, A Devresse, R Kettmann, N Simonis, F Dequiedt, and J C Twizere. Systematic interactome mapping of acute lymphoblastic leukemia cancer gene products reveals EXT-1 tumor suppressor as a Notch1 and FBWX7 common interactor. *BMC CANCER*, 16, 2016.

[90] Y Pakdaman, S Berland, H J Bustad, S Erdal, B A Thompson, P A James, K N Power, S Ellingsen, M Krooni, L I Berge, A Sexton, L A Bindoff, P M Knappskog, S Johansson, and I Aukrust. Genetic Dominant Variants in STUB1, Segregating in Families with SCA48, Display In Vitro Functional Impairments Indistinctive from

Recessive Variants Associated with SCAR16. *International Journal of Molecular Sciences*, 22(11):11, 2021.

[91] D K Guo, Z Ying, H F Wang, D Chen, F Gao, H G Ren, and G H Wang. Regulation of autophagic flux by CHIP. *NEUROSCIENCE BULLETIN*, 31(4):469–479, 2015.

[92] A Carnemolla, H Lazell, S Moussaoui, and G P Bates. In Vivo Profiling Reveals a Competent Heat Shock Response in Adult Neurons: Implications for Neurodegenerative Disorders. *PLOS ONE*, 10(7), 2015.

[93] T M Sonninen, G Goldsteins, N Laham-Karam, J Koistinaho, and S Lehtonen. Proteostasis Disturbances and Inflammation in Neurodegenerative Diseases. *CELLS*, 9(10), 2020.

A Appendix

A.1 Section selection for Purkinje cell count

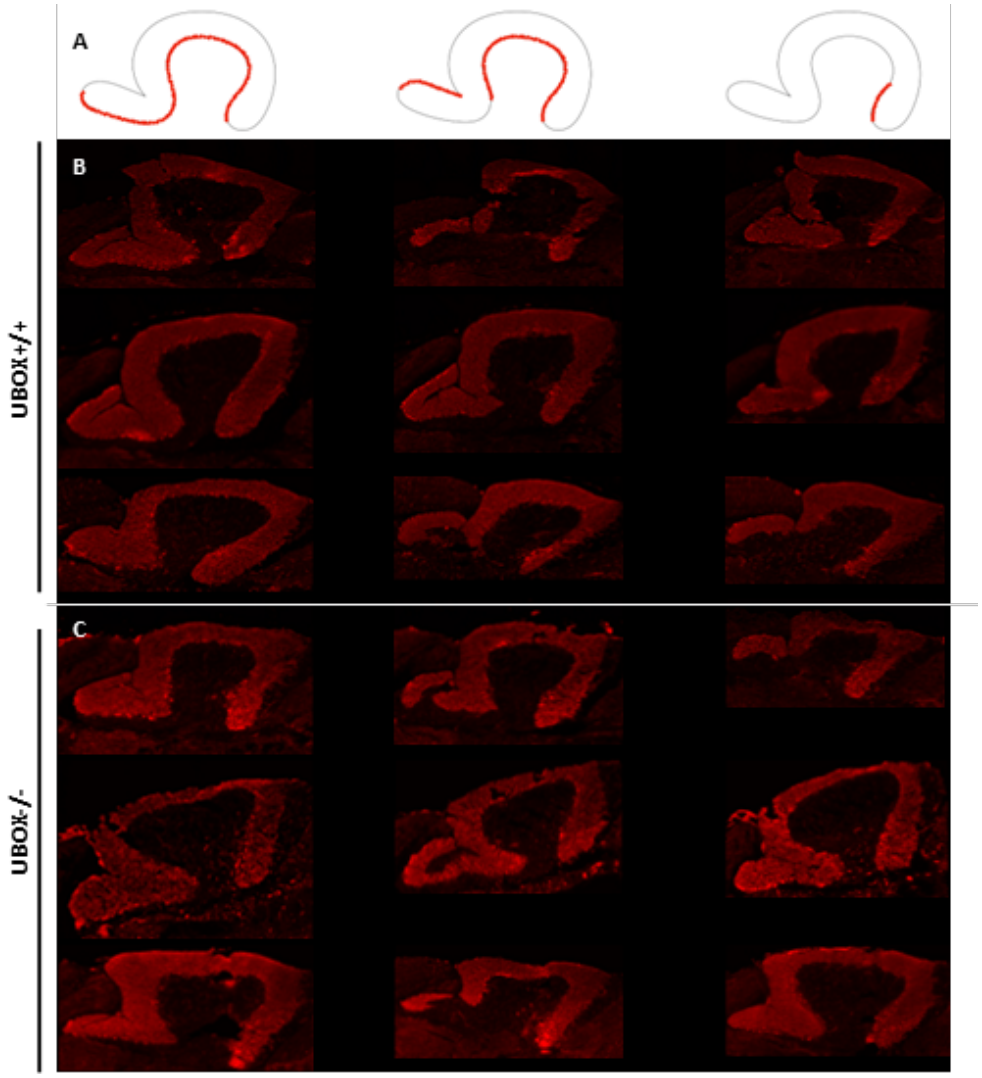

Figure A.1: ***Section selection for Purkinje cell count.*** *Parvalbumin stained brain sections of 3 year old zebrafish were scanned and three section for each individual were selected to contain Purkinje cells in the areas marked red (A). B shows the three wild-type samples, C shows the three mutants.*

A.2 Neurotracing reconstructions of all individuals in dendrite orientation analysis

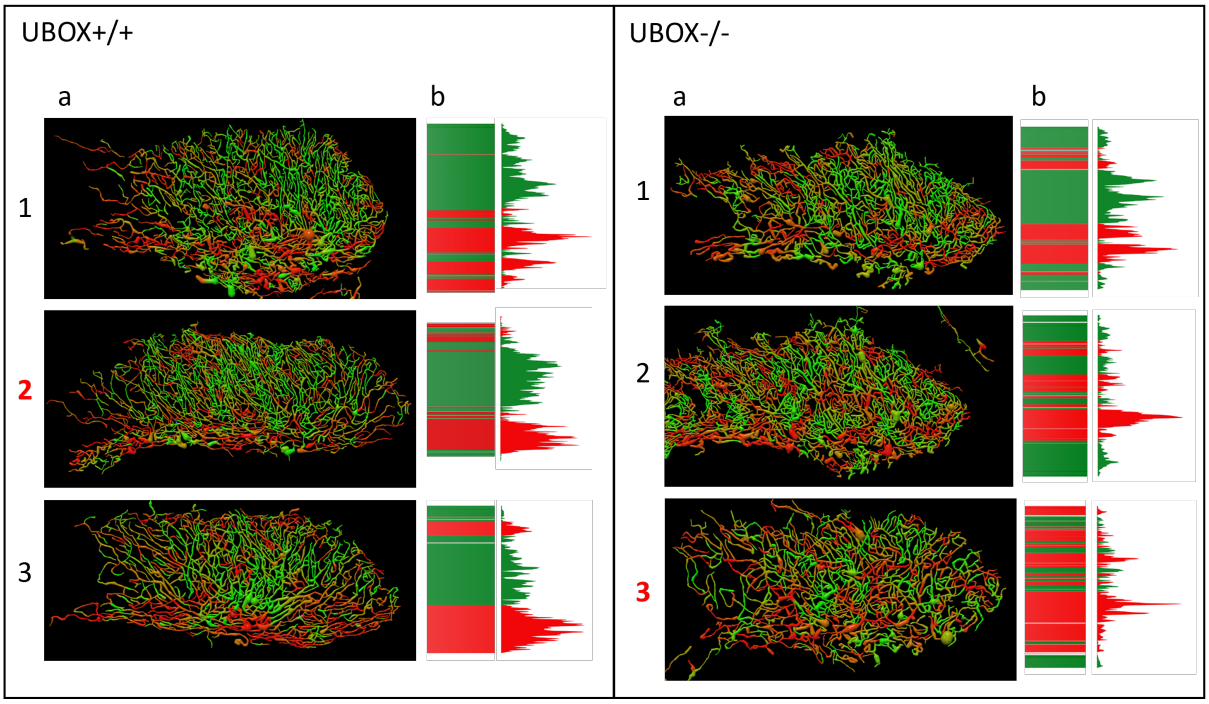

Figure A.2: ***Neurotracing reconstructions of all individuals in dendrite orientation analysis.*** *Neurotracing reconstructions (a) and quantifications of dendrite orientation (b) for UBOX+/+ individuals 1-3 are shown on the left, and for UBOX-/- 1-3 individuals to the right. The samples that are also presented in Figure 4.2 are marked with the red, bold font.*

A.3 RT-qPCR melting curves for primers and Ct values of all samples

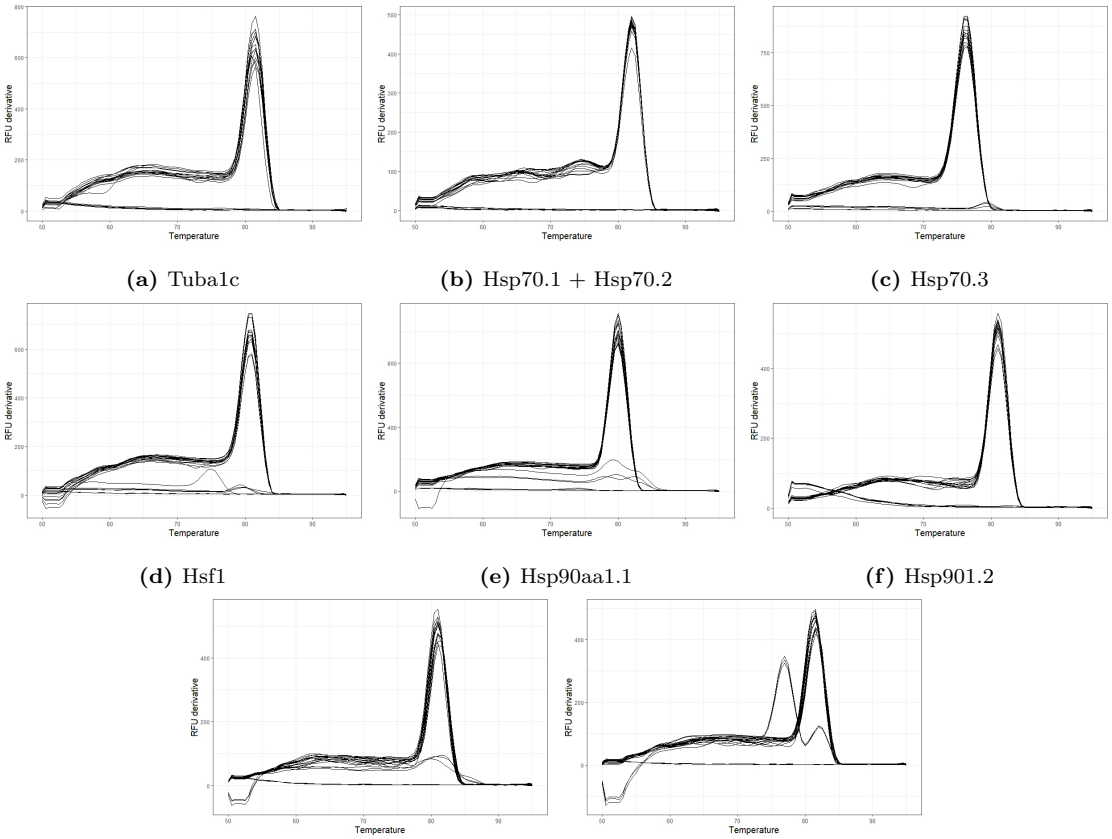

(a) Tuba1c **(b)** Hsp70.1 + Hsp70.2 **(c)** Hsp70.3

(d) Hsf1 **(e)** Hsp90aa1.1 **(f)** Hsp901.2

(g) Hsp90ab1 **(h)** Hsp90b1

Figure A.3: ***Melting curves for all RT-qPCR primers.*** *X-axis shows temperature, y-axis shows derivative of relative fluorescent signal (RFU).*

	tuba1c Ct values (2 replicates)		*hsf1* Ct values (2 replicates)		*hsp70.1 + hsp70.2* Ct values (2 replicates)		*hsp70.3* Ct values (2 replicates)		*hsp90aa1.1* Ct values (2 replicates)		*hsp90aa1.2* Ct values (2 replicates)		*hsp90ab1* Ct values (2 replicates)		*hsp90b1* Ct values (2 replicates)	
W60	22,71613	22,75589	25,203614	25,351254	27,126173	27,098139	26,862802	26,772616	23,294529	23,297084	22,843486	22,813064	18,433007	18,333313	23,122399	23,033738
W60	20,35840	20,35233	26,122865	25,626666	27,498846	27,499845	25,389246	25,529977	24,008437	23,90614	23,274023	23,337201	19,105911	19,028845	23,373274	23,384234
W60	22,18708	22,28662	24,818671	25,038056	26,919769	27,203366	26,483074	26,539145	23,338734	23,291895	22,586833	22,670435	18,299769	18,281307	22,651437	22,453413
W60	22,24419	22,36622	25,208644	25,185187	27,237657	27,291553	27,097673	27,207513	23,500506	23,737307	23,135729	23,255298	18,540456	18,479047	23,115997	23,115891
W60	21,42319	21,33321	26,578828	26,631298	27,706698	27,752394	26,208508	26,210296	24,426649	24,605387	24,291405	24,303994	18,867403	18,885899	23,752707	24,201312
W60	22,68894	22,70044	25,646573	25,465247	26,908451	27,381565	27,414387	27,589298	23,825726	24,416875	23,622962	23,694991	18,906779	17,583154	22,79664	23,060522
W120	22,21067	22,30460	24,433138	24,581913	27,967931	28,004909	28,098608	28,146201	24,597664	24,377009	23,259641	23,012436	18,702351	18,773167	22,333917	22,857627
W120	21,29543	21,90930	25,019091	25,101775	27,88591	27,911858	28,061731	28,088005	24,439256	24,341813	22,191207	22,778853	19,126989	19,237202	23,208852	23,201305
W120	20,67670	20,64916	23,381318	24,201376	28,719923	28,584494	27,357287	27,722866	23,284926	23,608221	23,263298	23,368032	19,575374	18,705359	24,120378	24,166257
W120	19,89711	20,29265	24,471242	24,451623	28,44076	29,617761	26,731856	27,101739	23,993427	24,925021	23,031741	23,905661	19,189183	19,402393	24,360112	24,716354
W120	20,67293	21,95556	24,392625	24,45722	27,58451	27,59193	26,229077	26,485673	23,617838	23,700119	21,641552	22,090312	18,862001	18,659055	22,474014	22,489175
W120	20,18214	21,02200	24,402214	24,41948	28,914449	29,479066	25,607424	26,648118	23,303344	23,556918	22,175644	23,476037	19,077066	19,556359	23,393108	24,508215
WH60	23,04077	23,14796	24,302769	24,306543	15,882957	15,682226	16,28179	16,477437	17,661108	17,585042	14,376374	14,325896	17,69693	17,694956	19,414986	19,330135
WH60	23,74913	23,82708	24,139305	23,93469	16,091076	16,038465	16,525422	16,65893	16,866892	16,762291	15,163861	14,167059	17,20174	18,088821	19,570623	19,622097
WH60	23,35795	23,52041	23,78259	24,721073	16,149103	15,959684	16,413159	16,529395	17,049955	16,698007	13,733668	14,268941	18,242067	18,185655	19,34136	19,337534
WH60	24,21185	24,42231	25,259687	25,020427	16,459656	16,450649	17,389877	17,359561	18,421155	18,140763	14,955265	15,005909	18,117625	18,054039	19,757271	19,822289
WH60	24,44634	24,41079	25,117948	25,072226	16,072191	16,070064	17,093126	17,080236	17,43547	17,51874	14,926629	14,986481	17,898271	17,881099	19,764585	19,850989
WH60	23,52924	23,62071	24,257898	24,270576	15,218129	15,33049	16,339614	16,494488	17,110457	17,371339	14,071986	14,167369	17,405788	17,497129	18,957559	19,050056
WH120	22,23004	22,39781	22,552483	23,294783	18,424687	18,348024	18,529056	18,684222	18,568192	18,562834	16,800473	16,806041	18,534487	18,465633	20,488257	20,427998
WH120	22,32889	22,10676	24,098899	24,120142	17,865351	17,813651	17,874338	18,606633	18,189835	18,130835	16,463064	16,32302	18,137711	18,154394	19,84344	20,006075
WH120	22,35227	22,45770	24,091556	24,155362	17,998896	17,810969	18,289925	18,857631	18,083199	18,158846	16,411385	16,445098	17,944402	17,999875	20,078802	20,085922
WH120	21,36169	21,80066	24,077105	24,108247	19,411112	19,650337	18,144764	18,761351	17,682732	18,272842	16,536095	17,182344	18,984556	18,848721	20,287056	20,587107
WH120	30,16120	30,70791	29,77094	30,3268	30,593694	30,881281	27,212732	27,753329	24,697195	24,616262	20,01207	20,318615	23,434964	23,745619	26,779936	27,369401

Figure A.4: ***All obtained Ct values from RT-qPCR for wild-type samples.*** *Two technical replicates were included, and the mean Ct values used for further calculations. Colours correspond to the boxplots in section 4.3.1.*

	tuba1c Ct values (2 replicates)		*hsf1* Ct values (2 replicates)		*hsp70.1 + hsp70.2* Ct values (2 replicates)		*hsp70.3* Ct values (2 replicates)		*hsp90aa1.1* Ct values (2 replicates)		*hsp90aa1.2* Ct values (2 replicates)		*hsp90ab1* Ct values (2 replicates)		*hsp90b1* Ct values (2 replicates)	
M60	22,51049	22,63747	26,131596	26,04908	26,734575	26,77724	27,438487	27,709344	24,355089	24,492125	22,758368	22,932139	18,133144	18,269704	24,105904	23,946224
M60	23,47987	23,56770	26,98032	27,022952	28,022818	28,064108	28,313373	28,764579	25,032269	25,302264	23,421389	23,710809	18,9924	19,230852	24,378918	24,79343
M60	21,46670	21,95371	26,510787	26,740253	27,528624	28,122197	27,226239	27,49102	23,368685	23,991002	22,716208	22,679531	19,187048	18,169786	23,902291	23,870798
M60	22,52323	22,27551	24,925131	25,499285	28,57375	28,645194	28,413624	28,555904	23,160779	23,955559	21,846606	22,325824	17,486178	18,780246	23,478805	23,554341
M120	22,57355	22,64569	25,640609	26,127393	27,797399	27,947416	26,496182	26,880784	24,299246	25,037116	22,035953	22,998487	19,556508	19,771051	24,914397	25,537544
M120	23,11683	23,29967	27,056361	26,885081	27,186405	27,036884	26,948118	27,126974	24,756412	24,842753	22,616336	22,784707	18,895043	18,931638	24,393474	24,368975
M120	23,05967	23,10076	25,800142	26,368755	27,585489	28,020337	27,111726	27,219937	23,572975	24,203473	22,820189	22,927656	18,718011	19,376325	23,977892	24,074755
M120	23,17741	23,19049	26,523213	26,536785	26,807794	26,762125	27,15083	27,127551	24,722189	24,86909	22,566594	22,504995	18,685998	18,767689	24,420428	24,289505
M120	22,49133	22,77945	25,685684	26,43086	27,075518	27,428036	26,598711	26,76113	24,454592	23,717331	20,881434	21,653982	18,461075	18,772419	23,490495	24,193339
M120	23,12599	23,13980	25,270118	26,149617	27,065419	27,080466	27,474917	27,416067	24,989723	25,024681	22,622895	22,766694	18,754915	18,897592	24,226753	24,264168
MH60	24,30439	24,72344	26,433801	26,257226	16,69589	16,734771	17,442406	17,612161	18,807917	18,846156	15,310496	15,401855	18,477309	18,415269	20,977302	20,737134
MH60	23,22353	23,33942	24,982821	25,524547	16,231686	16,220496	17,373769	17,352307	17,56129	17,578285	14,993473	15,013829	17,306717	17,306698	19,811788	19,783289
MH60	24,50178	24,63170	25,214026	25,221442	16,733609	16,683366	17,488255	17,465768	18,205796	18,469025	16,032071	14,736108	18,439818	18,631279	20,594814	20,690091
MH60	24,27568	24,27038	25,330394	25,327567	16,165563	16,136564	17,514012	17,441454	18,392903	18,325104	14,130787	14,590171	18,163426	18,259553	20,055967	20,071395
MH60	25,45147	25,68084	26,792581	27,001963	18,069722	18,082078	18,300847	18,368622	18,708891	19,081641	16,039421	15,431993	19,192089	18,830327	21,021382	21,736902
MH60	24,52020	24,51147	26,028579	26,199852	17,263478	17,330056	18,097907	18,147292	18,2675	19,291305	14,618536	16,959739	17,810471	18,385497	21,257865	21,267717
MH120	23,70959	23,88405	24,989216	25,051273	19,050017	18,779013	19,294546	19,61678	18,420664	18,662624	17,284621	17,099771	18,653212	18,107685	21,163703	20,96104
MH120	24,31007	24,56583	26,179071	26,148716	19,260983	19,27076	20,238977	20,514641	19,436095	19,489405	16,952609	17,017085	18,54585	18,70157	21,622001	21,709364
MH120	24,27364	24,37906	25,713986	25,67651	18,652219	18,488037	19,599461	19,508004	18,174389	19,701603	16,593733	16,962907	18,445364	18,797612	20,952488	21,049843
MH120	24,16341	24,21893	25,315685	25,307712	19,010588	18,72297	19,64436	19,663555	18,267532	19,008501	17,521156	16,819141	18,613871	18,806782	21,635306	21,531954
MH120	24,09374	24,15577	25,476813	25,304837	18,755219	18,665417	19,829315	19,85601	19,022107	19,068371	16,752	16,959338	18,30752	18,391639	21,013414	21,077535
MH120	23,77461	24,04202	25,068409	25,842278	18,329812	18,353549	19,542029	19,613147	18,814807	19,104566	16,587522	16,557311	18,149388	18,177624	20,857736	21,006199

Figure A.5: ***All obtained Ct values from RT-qPCR for UBOX-/- mutant samples.*** *Two technical replicates were included, and the mean Ct values used for further calculations. Colours correspond to the boxplots in section 4.3.1.*